



**Politecnico  
di Torino**

# **Simulation of multiphase transport of Dense Non-Aqueous Phase Liquid (DNAPLs) in a contaminated aquifer system**

**Masoud Zendegan**

**Collegio di Ingegneria per L'Ambiente e il Territorio**

Supervisor: Prof. Sethi  
Co-Supervisor : Dr. Bianco

November 2021

# Acknowledgement

This thesis was conducted to receive the Master of Science in Petroleum Engineering. First of all, I would thank my family for the unconditional support during my educational career. Likewise, I am pleased to carry out my thesis under the supervision of Prof. Dr. Rajandrea Sethi. At the end, I would thank also Dr. Carlo Bianco for his on going support as the Co-supervisor.

# Contents

<b>1</b>	<b>Introduction</b>	<b>1</b>
<b>2</b>	<b>Theoretical Background</b>	<b>4</b>
2.1	Aquifer Hydrogeological Scheme . . . . .	4
2.1.1	Principles of Hydrogeology . . . . .	4
2.1.2	Site Characterization . . . . .	6
2.2	Groundwater Contamination . . . . .	7
2.2.1	Phase Partitioning . . . . .	9
2.3	Mathematical Model . . . . .	10
2.3.1	Main Assumptions . . . . .	11
2.3.2	Governing Equations . . . . .	12
2.3.3	Thermophysical Properties . . . . .	15
2.3.4	Phase Equilibria . . . . .	17
2.4	Numerical Paradigm . . . . .	18
2.4.1	Space and Time Discretization . . . . .	18
2.4.2	Primary variable and Variable substitution . . . . .	20
2.4.3	Two and Three-Phase Capillary Pressures . . . . .	21
2.4.4	Newton-Raphson Iteration . . . . .	21
2.4.5	Boundary and initial conditions . . . . .	22
2.4.6	Appearance and Disappearance of Phases . . . . .	23
<b>3</b>	<b>Modelling approach</b>	<b>24</b>
3.1	Methodology . . . . .	25
3.1.1	Initialization and Boundary Condition . . . . .	26
3.1.2	Lithology and Mesh Gridding . . . . .	27
3.2	Run Segments . . . . .	28
3.2.1	Steady State Flow Condition . . . . .	28
3.2.2	NAPL Spill . . . . .	29

## CONTENTS

---

3.2.3	Monitoring NAPL Spread . . . . .	30
3.2.4	Pump and Treat Design . . . . .	31
3.3	Sensitivity Analysis . . . . .	31
3.3.1	Examined Parameters . . . . .	31
3.3.2	Scenarios . . . . .	33
3.3.3	Results . . . . .	42
3.4	Reference Scenarios . . . . .	50
3.4.1	Pipe Leakage . . . . .	50
3.4.2	Tank Spill . . . . .	55
<b>4</b>	<b>Conclusion</b>	<b>58</b>
	<b>Appendices</b>	<b>60</b>
<b>A</b>	<b>Appendix</b>	<b>61</b>

# List of Figures

2.1	NAPL phase partitioning at equilibrium . . . . .	10
2.2	Center-to-center distance and interface between grid block I and its neighbor m. . . . .	19
3.1	Sketch up design . . . . .	26
3.2	Standard 3-D model . . . . .	27
3.3	Steady state and hydrostatic pressure within the domain . . . . .	29
3.4	TCE spill. Slice view $v_{water} = 0.08$ m/day . . . . .	36
3.5	TCE spill. Slice view $v_{water} = 0.43$ m/day . . . . .	37
3.6	TCE yearly spill, $v_{water} = 0.9$ m/day . . . . .	38
3.7	PCE spill. Slice view $v_{water} = 0.08$ m/day . . . . .	39
3.8	PCE spill. Slice view, $v_{water} = 0.43$ m/day . . . . .	40
3.9	PCE spill. Slice view, $v_{water} = 0.9$ m/day . . . . .	41
3.10	the spatial evolution of the Yearly spill captured for $t_{seepage} = 1$ month and $t_{seepage} = 3$ month . . . . .	45
3.11	Area of influence for different injection rate . . . . .	46
3.12	High saturation zone( $S_{max}$ ) for different injection rate captured at $t_{seepage} = 1$ month . . . . .	47
3.13	The NAPL phase normalized volume for the Yearly spill captured for $t_{seepage} = 1$ month and $t_{seepage} = 3$ months . . . . .	48
3.14	TCE and PCE Monthly spill, $S_{max}$ vs $\log(t)$ . . . . .	49
3.15	TCE and PCE yearly spill, $S_{max}$ vs $\log(t)$ . . . . .	50
3.16	Hydrostatic pressure distribution in the system . . . . .	51
3.17	Pipe Leakage scenario. Distributed dissolved phase and NAPL position at the end of spill time . . . . .	52
3.18	Pipe leakage, $t_{monitoring} = 1$ year . . . . .	53
3.19	Pump and Treat Design, $t_{operation} = 6$ months . . . . .	54
3.20	Tank spill after seepage time, $t_{seepage} = 4$ days . . . . .	55

## LIST OF FIGURES

---

3.21	Tank spill spatial distribution at $t_{monitoring} = 1$ year . . . . .	56
3.22	P&T design, the spatial distribution of the NAPL pool at the bottom of the aquifer at $t_{seepage} = 4$ days . . . . .	57
A.1	Extraction of dissolved phase values cell by cell . . . . .	62
A.2	Extraction of saturation data from the output file of Petrasim Part I	63
A.3	Extraction of saturation data from the output file of Petrasim Part II	64

# List of Tables

3.1	Determined parameters for capillary pressure and relative permeability . . . . .	30
3.2	Physico-chemical properties of TCE and PCE . . . . .	32
3.3	the impact of different flow velocities and different chlorinated solvents on monthly spill spread . . . . .	42
3.4	The impact of different flow velocities and different chlorinated solvents on yearly spill spread . . . . .	43

# Chapter 1

## Introduction

As far as it is concerned, fresh groundwater has always been the primary source of the residential consumption, and in some degrees the feed for industrial activities as well. However, the over-consumption of the natural water resources for the industrial purpose has threatened the environment due to the release of harmful industrial by-products. During the recent decades, the industrial solvents<sup>1</sup> have been considered as a serious source of the groundwater pollution. Their low natural attenuation, i.e persistence in the natural environment, and toxicity brought a serious concern to the recovery of polluted sites. The synthetic hydrocarbons such as Trichloroethylene (TCE), Tetrachloroethylene (PCE) are the most detected Dense Non-Aqueous Phase Liquid (DNAPLs) that consequent environmental issues occurs when spilled into the fresh groundwater aquifer. Due to their high volatility and the carcinogenic impact of the inhaling or direct exposure, the remediation of the polluted sites requires great deal of effort. Indeed, reaching to an acceptable concentration of the aforementioned substances is essential for the regional water quality report. Corresponding to the Italian's law, the risk threshold concentration(CSC) for TCE and PCE are reported respectively  $1.5 \mu\text{g/L}$  and  $1.1 \mu\text{g/L}$  for residential site [8]. Note that the given concentrations for the residential site are taking into account the conservative approach. Furthermore, the spill of such substances into the aquifer results in the partitioning of the contaminant within different phases of the porous system. Basically, the formation of non aqueous phase as a separated phase in the aquifer is more likely to happen. Consequently, the migration path

---

<sup>1</sup>Chlorinated Hydrocarbon by products.

---

of the spill is required to be detected. However, the presence of irregularity in heterogeneous subsurface leads to the formation of the preferential pathways. Thus, it is required to understand the site hydrogeological features and the physico-chemical mechanisms of the hydraulic system. Normally, the dynamic spreading behavior of the DNAPL spill is modelled based on the computation fluid dynamics(CFD) principle. Several well survey, field observation and well logging tool should be necessarily carried out for the proper characterization of the polluted site. Importantly, the calibration of the natural flow system necessitates the better understanding of the hydrogeological parameters.

Once contaminant is present in the aquifer system, the multiphase controlling parameters are key to be calibrated before running the desired model. Theoretically, the higher density of the DNAPLs predicts the downward movement of the substances and creating of pools in the aquifer bed. Consider that the NAPL phase behaves as secondary source for generation of the dissolved phase into the aquifer. Consequently, the generation of dissolved contaminants within the aqueous phase continues until the removal of the NAPL phase takes place. Ultimately, the quantification of the relevant volume which is contaminated by NAPL phase or dissolve phase are presumed essential when it comes to the remediation of the polluted site.

Altogether, this study has first described the site characterization criteria and the theoretical background behind the physicochemical processes governing the multiphase flow dynamic in porous system. Afterward, the procedure for modelling of the DNAPL spill problem has been elaborated by segregation of the problem into several simulation phases to incorporate the proper modelling of the scenario. Through the sensitivity section, modelling scenarios has discussed the spatio-temporal evolution of the spill in shallow underground aquifers under different hydrogeological setups and anthropogenic parameters. The previous studies have targeted the influence of the groundwater velocity on the spill spreading behaviour [7]. Followingly, this study has examined the sensitivity of three parameters: **Ground water velocity, Spill time, and Different chemical solvent.**

Afterwards, the reported results are applied for the design of pump and treat field on two reference scenarios with the aim of embedding the real spill incident in the simulation study. Correspondingly, two most probable spill incident of pipe leakage and tanker spill are studied. Importantly, the position of the generated NAPL pool in the bottom of the aquifer is key tool to find the best position for the pumping well. Therefore, the topography

---

of the aquifer bed has been extracted via Sketch up design tool. Note that several data inspection processes are carried out to demonstrated the capability of the software in quantification of relevant parameters. Supposedly, the introduced parameters are to enlighten new aspects of multiphase flow dynamic behavior. The data processing is carried out by Python with the aim of data extraction and applied data sorting approach. The procedure has been employed to quantify the volume of the aquifer which is occupied by either dissolved phase or NAPL phase,. Through that, the result has been reported to show the versatility of the implemented software for the purpose of NAPL spill modelling.

The simulation study has shown certain level of reliability to predict the spill dynamic behavior under different hydro-geological setup and the applied remediation technology, i.e Pump and Treat technique. The modelling of the system has been carried out with Petrasim software, based on TOUGH-code family [19].

# Chapter 2

## Theoretical Background

### 2.1 Aquifer Hydrogeological Scheme

The fundamental role of the underground freshwater in the daily life of human beings has always been noticed. However, the industrial pollution into the groundwater system has resulted in a global health concern and consequently a drastic shortage of natural water resources. Therefore, the geology science has been considered as a first hand tool which contributes to the understanding of the underground water system. In the following sections the hydrogeological features of the system has been detailed. Afterward, the contamination physico-chemical interactions with the subsurface is explained based on the phase partitioning phenomena. At the end, the mathematical formulation of the phenomena governing the flow dynamic in the aquifer system is summarized for better understanding of the code implemented by the software.

#### 2.1.1 Principles of Hydrogeology

The geology science has enlighten the basic principles of the hydraulic cycle within the saturated subsurface layers. Consequently, The interrelation of underground water with the surface water has also been considered as a helpful tool to enrich the understanding of underground flow oscillations, i.e charges and discharges. Although the hydrologist may focus more on the characterization of the aquifer system than dealing with the water budget of the system. Indeed, dealing with the relevant factors such as hydraulic conductivity, boundaries, matrix structure and the lithology of the sub-surfaces

## 2.1. AQUIFER HYDROGEOLOGICAL SCHEME

---

are of their interest. However, It is ascertained that the geological history of the site has key role in the primary and secondary formation of the Hydrogeological setup. For instance, the formation texture controls the physico-chemical potential of the formation. Additionally, the reactivity of the soil materials with the contaminants is controlled by ion exchange capacity of the soil particles.

Meanwhile, for the scope of study, the evaluation of the runoff amount, i.e interchange between surface stream and groundwater flow, has been listed below [6]:

1. Groundwater runoff.
2. Surface runoff.
3. Regional groundwater recharge rates.
4. Determination of areas of relatively high permeability or water-yielding characteristics.
5. Determination of background concentration of the groundwater quality.
6. Estimation of evapotranspiration.
7. Determination of the percentage of precipitation that is evapotranspired, becomes groundwater runoff, or becomes surface-water runoff.

Taking into account the different approaches, quantification of the run off amount has been studied either locally or regionally [6]. Practically speaking. the data survey is essential to be addressed in either small or large scale domain.

In order to compare the annual recharge and discharge of the groundwater stream, the hydro-graph data is required to be applied [3]. In fact, the head variation due to the seasonal change is of importance when it comes to the regional study of the field. However, the examination of topography and geology of the field are crucial in the run off amount.

Furthermore, the application of depletion curve enlightens the aquifer hydraulic potential and characteristics of the groundwater reservoir, although the target of this study has assumed a confining shallow aquifer. In this case, the potentiometric surfaces, i.e imaginary head value where a given reservoir will equalize out to, is applied. Introducing a suitable set of hydrogeological parameters is essential for the proper modelling of water system [3].

### 2.1.2 Site Characterization

Basically, the remediation of underground water system are consequence of a failed project. Therefore, a feasible trade-off between time and cost has always been considered before initiating any remediation technique [13]. Accordingly, the background knowledge of the site is a valuable tool for the primary assessment of the risk and hazard index. The work flow for implementing the remediation technique to a polluted site undoubtedly urges the calibration of the hydro-geological parameters. Note that the site characterization has significant contribution to time and cost of the operation.

In fact, The most reliable method for the hydrodynamic characterization is well survey [5]. Basically, the external perturbation, i.e. change in pressure of the pump, provides practical data from the subsurface hydraulic frame. The measured parameter is the change in water level, i.e. drawdown( $s$ ), in the well which is caused because of the cone depression around the well bore area. The data observation can be either in the same well or other monitoring wells [11]. Even though well testing provides a great deal of accuracy for the system parameters, other techniques such as lab measurement or empirical correlation can be replaced when it comes to the cost of the operations.

Technically, the hydrodynamic characterization of the site provides following information

1. The hydraulic typology of the aquifer, which is obtained by the well data [11]. Whether the aquifer is confined, semi-confined or unconfined. The procedure is to analyse the drawdown value during the time evolution of the pressure perturbation.
2. The hydrodynamic parameters such as porosity, and hydraulic conductivity of the porous media which are controlled by the stratigraphy of the saturated layer and particle size distribution of the soil grains. In addition, the storativity of the confined aquifer is related to the compressibility of the water and porous matrix. Generally, the incompressible fluid is assumed for the purpose water system modelling [12]. Meanwhile, the expansion and compaction of the system has been embedded into modelling by means of suitable factors [19].

## 2.2 Groundwater Contamination

The quality of the water while having its hydrologic cycle alters. The natural and anthropogenic changes in the water composition is needed to be addressed to satisfy the residential or industrial standard of the water quality. Unfortunately, many of the industrial wastes has been disposed in the fresh water underground cycle and subsequent increase in the toxicity index of the water has been observed .

The chlorinated solvents are the most detected industrial wastes which are found nearly within all the industrial sites. These extremely toxic chemical compounds are synthetic hydrocarbons, in which the Chloride is bonded to the Carbon atom. Therefore, the persistence of the substance in the environment is relatively high. In other words, the natural attenuation of the substance is low. Following the half-life time principle, e-folding time for these substances are considered 10 up to 20 years [21]. It is better to remind that, due to the absence of the air below the water table, the natural attenuation of the substance by microorganisms can not properly take place. Thus, following the Italian environmental law, a pragmatic approach is required to decrease the concentration of the mentioned substances to the order of  $\mu\text{g/L}$ . First of all, the physico-chemical properties of the substances are required to be addressed. For that, several data survey has been carried out to forecast the spreading mechanisms of the pollution within the aquifer system. In term of the chemical properties, the chlorinated solvents are hydrophobic substances, therefore their solubility in the water is quite low. Despite their low solubility, even small fraction of the mentioned substance in the aqueous phase give rise to serious health problems.

Evaluating the kinematic parameters of the contaminants, their density is higher respect to water. Consequently, the downward movement of the substances in the aquifer system is expected. Moreover, generation of the NAPL pool along the bed is likely to happen when excessive amount of the substance distributed in the medium. Better to keep in mind that the artificial pumping of water in the residential sites leads to preferential flow pathways as result of the produced depression cone around the pumping well [15].

There are four major controls which are introduced to the shallow groundwater contamination [6]. As it is discussed earlier, the first control parameter is the physical and chemical features of the earth materials, see Section (2.1.2). The second major control factor is the natural processes that take place either by fluid-rock interaction or fluid-fluid interaction. the aim of the nat-

## 2.2. GROUNDWATER CONTAMINATION

---

ural processes are to recover the equilibrium of the natural potential of the environment. The following processes are most probable to happen in the subsurface by means of removing or degrading the pollution [22]:

1. **Filtration.** In response to the contamination spill, the porous matrix acts as resistant to the spread of the pollution by trapping the substances in inter-granular spaces available for the flow. Additionally, the capillary pressure is considered as a controlling parameter on the dynamic behavior of the spill in the water saturated domain.
2. **Sorption.** Certain amount of the pollution phase physically or chemically reacts with the solid grains, which results in the sorption process. Hence, the fluid-rock interaction should be quantified by assuming a suitable isotherm. Note that the proper choice of isotherm takes into account the type of contamination whether it is organic or non-organic compound. Generally, for the organic pollution, the linear isotherm is a reliable tool to model the sorption phenomena.
3. **Ion-Exchange.** The soil has been usually assumed to be negatively charged due to the structural body and the elements which are presented in the soil. The valence number of the elements determines the strength of the cation exchange capacity(CEC), i.e soil ion-exchange potential. However, the ion-exchange takes place with a relatively slow process. For that reason, the contact time of the fluid and rock soil is of importance to be considered when it comes to the remediation of the polluted soil.
4. **Dispersion.** Following the *Fickian's Law*, the kinematic dispersion causes molecular diffusion and velocity gradients. The front of the dispersion wave is function of the water saturation [6],
5. **Aerobic or Anaerobic degradation.** The air presence in the superficial soil significantly contributes to the aerobic degradation of the contaminants. Note that the nutritional need of the microorganisms should be satisfied for a reliable degradation process. Practically, the reaction occurring in the subsurface is redox reaction [12]. therefore, the redox potential of the system is required to be evaluated. the less redox potential environment tends to degrade the substances by employing different elements such as  $Fe^{(II)}$  or  $Fe^{(III)}$ , specially at deep subsurface layers, providing anaerobic degradation processes, due to the lack of air [23].

## 2.2. GROUNDWATER CONTAMINATION

---

The third factor is how the spill has been introduced to the hydraulic flow system. Indeed, the way in which the spill penetrated or passed through, generates different spill scenarios. For instance, the contaminant may flow through aquifer directly, or through inter-aquifer leakage, amount of spill in the span of time and etc [1]. Lastly, to a large extent, the aquifer framework determines the flow dynamic and spill distribution.

For that reason, the previous studies has shown strong influence of the groundwater velocity in the distribution of the NAPL phase within the aquifer system. Likewise, this study not only targets the water velocity, but also examines the effect of the hydrogeologic and anthropogenic parameters in the dissolution and distribution of NAPL phase. In the Section (3.3) the details of the scenarios has been elaborated.

### 2.2.1 Phase Partitioning

The contaminant phase tends to reach to the equilibrium by distribution through other phase existed in the aquifer system, i.e water and solid matrix. Generally, in some shallow aquifers the presence of the air has been confirmed as well. the contaminant may dissolve either in the water or in the air. Likewise, it may adsorpted by the soil grains. if a noticeable amount of pollution introduced to the aquifer system, then the presence of non aqueous phase would be expected. In this case, the removal NAPL is the first step, since it produces continuous dissolved phase in the water.

Presence of multiphase within the porous system brings the application of capillary pressure and the relative permeability of the phases. Studies shows that pressure difference within the phases can be formulated based on the difference in the saturation values of them [16]. In fact the capillary pressure becomes significant when there is huge difference between the saturation values of the phases. Therefore, it is required to be properly modeled. Moreover, the introduction of multiphase flow to the porous system decrease the available flow section for the phases. In order to address that, the previous experimental studies have related the relative permeability of the phases to their saturation. These two parameters build the basic of multiphase flow in porous system. Thus, understanding the dynamic behavior of the system requires proper assumptions to build an efficient model.

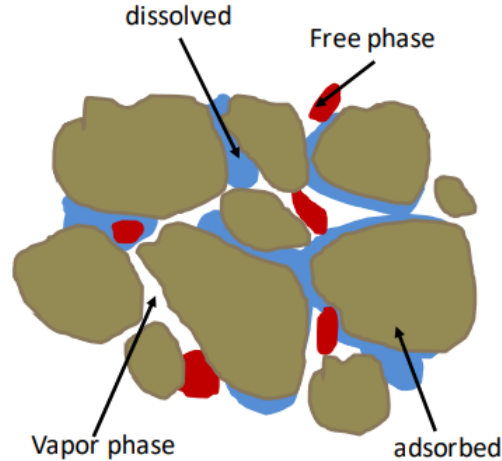


Figure 2.1. NAPL phase partitioning at equilibrium

The figure (2.1) presents the possible pollution phases existing in the aquifer system. Since the study targets the volatile organic compounds, the volatility of the NAPL phase is of importance to be properly modeled [20], which is addressed by suitable equation of states (EOS). Taking into account that, the vapor pressure of the component is a key parameter to determine the solubility into the air and water at equilibrium. The difference in the physical properties and structures of the components, i.e. water and contaminant, necessitated the application of *Henry's law*. Basically, at a given vapor pressure, the concentration of the components in the liquid phase is assumed constant [5].

Better to note that, the phenomena occurring in the aquifer-NAPL multi-phase system is not limited to physico-chemical processes. the natural degradation mechanism is another control factor which is describing the fate of the pollutant distributed into the aquifer. In the next section, the mathematical modelling of the system has been detailed including all physically, chemically, and naturally phenomena governing the system dynamic behavior.

## 2.3 Mathematical Model

Petrasim implements the TMVOC numerical simulator to perform three-phase non-isothermal flows of multicomponent hydrocarbon mixtures in sat-

### 2.3. MATHEMATICAL MODEL

---

urated heterogeneous media. The broad application of the simulator is to analyze the fate and transport of non-aqueous phase liquids (NAPLs) in the vadose zone as well as below the water table [19].

the software incorporates the different thermodynamic conditions, advective-diffusive flow behavior, phase-partitioning, and sorptive processes. The natural attenuation of the substances has been modeled by the simple half-life time principle. In the TMVOC formulation, the multi phase system is assumed to be composed of water, non-condensable gases (NCGs), and water-soluble volatile organic chemicals (VOCs). In the most of the cases, air will be present as the single NCG within the aquifer system. The volatile organic compounds (VOCs) in this case has been selected TCE and PCE as common industrial solvents which are found near almost all the chemical industries. It is ascertained that the NAPL migration is governed by the density, viscosity, its quantity and the rate of release [1]. The mentioned simulator has embedded flow of all three fluid phases in response to viscous, gravity, as well as capillary forces. It is employed to model the transport phenomena in one, two, or three space dimensions with arbitrary geometry. The compositional characteristic of the simulator has facilitated the thermodynamic variation of components within the system. The partitioning of a component among the phases is calculated from the assumption of local equilibrium. Moreover, the various mass transfer mechanisms including evaporation and condensation of NAPL components and water, dissolution of NAPL into the water phase, and Henry's law partitioning of chemical components between the water and gas phases has been taken into account. The solid-liquid interaction, i.e. adsorption of contaminant has been included as well. Additionally, the heat exchange criteria is also accounted for [1].

The flow module of TOUGH-code family is written based on the general mass balance equation of an arbitrary number of components distributed among any number of phases. The thermophysical properties of the phases, e.g. density, viscosity, enthalpy, and mole fractions have been considered as the required input parameters to calculate the flux and the accumulation terms [18]. The mathematical formulation of the physicochemical mechanisms governing the natural environment has been elaborated by the following section.

#### 2.3.1 Main Assumptions

In order to characterize the aquifer system, the following assumptions have been made to develop the code functionality [1]:

### 2.3. MATHEMATICAL MODEL

---

- Darcy flow has been considered to describe multiphase flow in the porous media.
- Local chemical and thermal equilibrium has been assumed for the simplicity of the thermodynamic variation within the system.
- For the molecular diffusion, constant diffusion coefficient has been applied.
- Linear adsorption isotherm characterizes the rock and fluid interactions.
- The energy variation due to the acceleration and viscous dissipation is overlooked.

#### 2.3.2 Governing Equations

The multicomponent fluid flow equation has been described by the conservation of mass, Darcy's law, and conservation of thermal energy, taking into account non-isothermal condition:

$$\frac{\partial}{\partial t} \left[ \frac{(1 - \phi) \rho_r w_{ir}}{M_i} + \phi \sum_{\beta=w,o,g} S_\beta \rho_\beta x_{i\beta} \right] = -\nabla \cdot F + q_i \quad (2.1)$$

Where the subscriptions w, o, g describe the three phases within the flow system,  $\phi$  represents the effective porosity, i.e excluding the dead-end flow paths and isolated void space within the rock matrix (2.12);  $F$  is the molar flux, the sink or source term has been quantified by term  $q_i$ ,  $\rho_r$  is the density of the matrix,  $w_{ir}$  is the adsorbed mass of component i per unit mass of rock grain,  $M_i$  is the molecular weight of the component i;  $S_\beta$  indicate the saturation of the relevant phase in the system,  $\rho_\beta$  is the phase molar density and  $x_{i\beta}$  is the mole fraction of component in phase  $\beta$ .

As is shown in (2.1), the hydrodynamic dispersion has not been included in the formulation, i.e Fickian law [1].

The molar flux term,  $F_i$ , has been developed by Darcy law of multiphase fluid flow in porous media:

$$F_i = - \sum_{\beta=w,g,o} \left[ x_{i\beta} \rho_\beta \frac{K k_{r\beta}}{\mu_\beta} \cdot (\nabla P_\beta - \rho_\beta g) + \phi S_\beta \tau_\beta \rho_\beta D_{i\beta} \cdot \nabla x_{i\beta} \right] \quad (2.2)$$

### 2.3. MATHEMATICAL MODEL

---

Where  $K$  is the intrinsic permeability which is controlled by the particle size distribution of the inter-granular space[18];  $k_{r\beta}$  is the relative permeability of phase controlled by the saturation profile and residual saturation for the phases (2.6). The residual saturation indicates the threshold residual amount of the phase which it can keep the continuous pressure gradient along the flow path.  $\mu_\beta$  is the viscosity of the phase,  $\tau_\beta$  represents the tortuosity of the porous system, i.e complexity of the flow paths within the medium.  $D_{i\beta}$  is the diffusion coefficient tensor of component  $i$  in phase  $\beta$ , which has been applied as a constant value for the simulation purpose. Substituting the Eq (2.1) and (2.2), the thermal energy transfer has been described by

$$\begin{aligned} \frac{\partial}{\partial t} \left[ (1 - \phi) \rho_r C_{Pr} T + \phi \sum_{\beta=w,g,o} S_\beta \rho_\beta U_\beta \right] \\ = \nabla \cdot \left[ \sum_{\beta=w,g,o} H_\beta \rho_\beta \frac{K k_{r\beta}}{\mu_\beta} (\nabla P_\beta - \rho_\beta g) + \lambda \cdot \nabla T \right] + q_{heat} \quad (2.3) \end{aligned}$$

As it is shown, the equation controls the conduction and convection parameters, where  $T$  is the temperature,  $C_{Pr}$  is the rock grain specific heat capacity which in the simulation has been considered same as the wet rock;  $U$  presents the molar internal energy of phases,  $\lambda$  is the effective thermal conductivity tensor of the porous system,  $H_\beta$  is the molar enthalpy of the phases present within the aquifer system, and  $q_{heat}$  as a source or sink term, takes into account the heat generation flux per unit of porous volume. Notice that the diffusive heat flux has been neglected.

The auxiliary equations which are required to characterize the system have been provided with the interrelation parameters that govern the dynamic behavior of the system [1]:

1. Phase saturation has to reach to the unit value:

$$\sum_{\beta=w,o,g} S_\beta = 1 \quad (2.4)$$

2. Mole fraction of the components in each phase sums to unity:

$$\sum_{i=1}^N x_{i\beta} = 1 \quad \beta = w, o, g \quad (2.5)$$

### 2.3. MATHEMATICAL MODEL

---

3. Relative permeability of the phases is function of the saturation:

$$k_{r\beta} = k_{r\beta}(S_w, S_g, S_o) \quad \beta = w, g, o \quad (2.6)$$

For the simulation of NAPL spill, in this study, nonlinear *Stone's three-phase model* has been recommended by the author for the multi-phase flow in the groundwater system system [22].

4. Capillary pressure has been employed as function of the saturation profile hence:

$$P_{cow} = P_o - P_w, \quad P_{cow} = P_{cow}(S_o, S_g, S_w) \quad (2.7)$$

Meanwhile the Parker experimental setup has given more accuracy to forecast the pressure variation within the phases [16].

5. Adsorption phenomena has been applied as linear isotherm with a constant coefficient  $K_D$ :

$$w_{ir}/w_{iw} = K_D(T) \quad (2.8)$$

Where the  $K_D$  constant is function of Total Organic Compound (TOC) of the soil and octane-water partitioning coefficient[10],  $K_{oc}$ :

$$K_D = f_{oc}K_{oc} \quad (2.9)$$

6. phase densities, internal energies, enthalpies and viscosities are function of temperate, pressure, and phase composition[1]:

$$\rho_j = \rho_j(P, T, x_{1j}, \dots, x_{Nj}), \quad j = 1, 2, 3 \quad (2.10)$$

7. Assuming the equilibrium of all chemical components partition phase among all the phases:

$$\frac{x_{iw}}{x_{ig}} = K_{iwg}(P, T, x_{iw}, x_{ig}), \quad K_{iog} = \frac{K_{iwg}}{K_{iwo}} \quad (2.11)$$

The porosity of the porous media is assumed variable due to pressure and temperature oscillation:

$$\phi_{eff}(P, T) = \phi_{eff}(P_{int}, T_{int})[1 + \epsilon_P(P - P_{int}) + \epsilon_T(T - T_{int})] \quad (2.12)$$

### 2.3. MATHEMATICAL MODEL

---

In which the subscript *int* indicates the initial condition of the thermodynamic parameters, applying the concept of expansivity and compressibility of the pore [19], to account for the expansion and compaction of the system, i.e Hysteresis effect. Thus, "no Stress" criteria, i.e overlooking the subsidence of the formation, is introduced to the system.

8.  $\lambda$  in the heat exchange formula has been assumed as function of phase saturation within the System. However, in this study the Heat exchange has minor importance in the dynamic of the NAPL spill into the aquifer media:

$$\lambda(S_w, S_o, S_g) = (1 - \phi)\lambda + \phi S_l I \lambda_w \quad (2.13)$$

Where I is the identity tensor;  $S_l$  presents the total saturation of the liquid phase. The previous studies has shown that the gas saturation within the system has negligible effect on the thermal conductivity of the rock matrix [17].

9. Tortuosity of the gas flow has been functioned based on porosity and gas saturation:

$$\tau_g(\phi, S_g) = \phi^{1/3} S_g^{7/3} \quad (2.14)$$

Accordingly, the simulator has embedded that as an input parameter to adjust the suitable value for the complexity flow through the interconnected pores [14].

#### 2.3.3 Thermophysical Properties

Thermodynamic variation of system has been modeled based on the cubic equation of state (EOS). In order to have a wide range of pressure and temperature condition accessible in the data base, the below simplifications has been listed:

1. **Gas phase.** The gas phase includes a broad spectrum of hydrocarbon chains, and consequently raises the complexity to deal with the mixture gas phase. However, for the further simplification, several experimental equations has been applied to reasonably decrease the complexity of

### 2.3. MATHEMATICAL MODEL

---

the phase thermodynamics. The applied equation for describing the thermodynamic behaviour of the gas mixture is *Saove and Redlich and Kwong* equation of State(EOS):

$$Z^3 - Z^2 + (A^* - B^* - (B^*)^2)Z - A^*B^* = 0 \quad (2.15)$$

Where  $A^*$  and  $B^*$  has been implemented by the justified experimental results for the gas phase which is the mixture of two or more chemical components [20].

As soon as the compressibility factor,  $Z_g$ , for the gas mixture is known, the density of the phase will be an input parameter for the fluid flow analysis. Moreover, the enthalpy of the gas phase has been comprised of two parts: enthalpy of water vapor within the gas mixture, and enthalpy of air-hydrocarbon fraction of the gas, which the software aligned with that [19].

The viscosity of the gas mixture is modeled using the Analytical method of *Wilke*, as function of temperature, pressure, and composition:

$$\mu_g = \sum_{i=1}^N \frac{x_{ig}\mu_i}{\sum_{j=1}^N x_{jg}\Phi_{ij}} \quad (2.16)$$

In which the simulator evaluates the both components as a single pseudocomponent, and brings out a desirable output.

2. **Oil Phase.** Considering the NAPL phase as slightly compressible fluid, the phase density is function of temperature and the composition. The enthalpy of the liquid phase whether vaporization or condensation has been formulated and embedded in the simulator. Importantly, in the non-isothermal condition, it plays a significant role in phase partitioning phenomena. Afterwards, the vapor pressure of the phase has been calculated by Wagner equation [20]:

$$P_{vap} = P_c \exp[a(1 - T_r) + b(1 - T_r)^{1.5} + c(1 - T_r)^3 + d(1 - T_r)^6/T_r] \quad (2.17)$$

Where the output value is function of critical temperature,  $T_r$ , assigned for the hydrocarbon mixture in the liquid phase. On the other hand,

### 2.3. MATHEMATICAL MODEL

---

in most cases the accuracy required for the vapor pressure value is satisfied with Antoine correlation:

$$\ln P_{vap} = A - \frac{B}{T + C} \quad (2.18)$$

Where A, B, C are empirical values which listed over hundreds of components[20]. The viscosity has been presumed as function of temperature with the following equation:

$$\ln \mu = A' + \frac{B'}{T} + C'T + D'T^2 \quad (2.19)$$

Which is obtained from the experimental setup carried out for several organic compounds [24].

3. **Water Phase.** The water thermodynamic condition has been assumed independent of the dissolved NAPL phase, due to the low solubility in water. Consequently, the water physical properties are only presumed to be function of temperature and pressure.

#### 2.3.4 Phase Equilibria

To satisfy chemical equilibrium criteria, the chemical potential of the each component should be equal in all phase, which simply saying that the effective pressure, fugacity  $f$ , is required to be equal.

$$f_{iw} = f_{io} \quad f_{iw} = f_{ig} \quad f_{io} = f_{ig} \quad (2.20)$$

Where  $f_{iw}$  indicate the fugacity of component i in water phase. In addition, the fugacity of componet i in liquid phase is related to the mole fraction of i in that phase following the fugacity equation:

$$f_{iw} = x_{iw} \gamma_{iw} f_i^R \quad f_{io} = x_{io} \gamma_{io} f_i^R \quad (2.21)$$

Where  $\gamma_{io}$  and  $\gamma_{iw}$  are the fugacity coefficients of i in the water and oil phases, respectively  $f_i^R$  is the reference fugacity of the pure liquid i at the temperature of the system [1].

In order to calculate the phase equilibria, the following assumption has been made:

## 2.4. NUMERICAL PARADIGM

---

1. Unity value has been assumed for the fugacity coefficient  $\gamma$ , i.e an ideal mixture of NAPL.
  2. In the ideal gas mixture, the partial pressure of a component is equal to the fugacity.
- (a) **Water-oil equilibrium.** Considering (2.20), (2.21) and  $\gamma_{io} = 1$ , achieving to:

$$x_{io} = x_{iw}\gamma_{iw} \quad (2.22)$$

The constant fugacity coefficient has been assigned due to the low solubility, i.e low solute-solute interactions. Therefore, the fugacity coefficient can be simply calculated as inverse of the mole fraction in water at the solubility limit  $\gamma_{iw}^{sol}$ . Solubility of the compound is present following the below equation [1]:

$$x_{iw} = a + bT + cT^2 + dT^3, \quad (2.23)$$

Where a, b, c, d has been obtained by fitting the experimental data.

- (b) **Water-gas equilibrium.** Using equation 2.20 and taking into account the first simplification, i.e  $\gamma = 1$ :

$$P_i = (P_{vap,i}/x_{iw}^{sol})x_{iw} \quad (2.24)$$

Where  $P_i$  is the partial pressure of the component i. the formulation model basically is elaborated by Henry's law, in which the  $P_{vap,i}/x_{iw}^{sol}$  is equal to Henry's constant. Therefore the equilibrium constant between the phase is calculable:

$$K_{iwg} = \frac{x_{iw}^{sol}}{P_{vap,i}}P \quad (2.25)$$

- (c) **Oil-gas equilibrium.**  $K_{iog}$  can be calculated as  $K_{iwg}$ , and  $k_{iwo}$  are known due to the equation (2.11).

## 2.4 Numerical Paradigm

### 2.4.1 Space and Time Discretization

The numerical algorithm used to handle the space and time intervals is IFDM method, i.e Infinite finite difference method. Therefore, the modeler is able to

## 2.4. NUMERICAL PARADIGM

---

introduce an arbitrary shaped polyhedrons by means of connecting the nodal points. This advantage of the mentioned method enhances the feasibility of the properly performing numerical simulation within an arbitrary domain. The spatial and time variation of the system can be robustly calculated through the IFDM method of discretization. Respectively, the IFDM form of the mass conservation equation has been discretized over an arbitrary finite flow domain of  $l$  with volume of  $V_l$ . Applying the divergence theorem to (2.1) and (2.3):

$$\int_{V^l} \frac{\partial}{\partial t} \left[ \frac{(1-\phi) \rho_r w_{ir}}{M_i} + \phi \sum_{\beta=w,o,g} S_{\beta} \rho_{\beta} x_{i\beta} \right] dV = \int_{\Gamma^l} \vec{n} \cdot F_i dA + \int_{V_l} q_i dV \quad (2.26)$$

Where  $F_i$ , molar flux, has been given following the multi phase Darcy's law and diffusive term (2.2);  $\Gamma^l$  is the bounding surface of  $l$ , and  $n$  is the outward unit normal vector [1].

The source or sink term represents the net rate(moles per unit time) at which the component  $i$  leaves the volume element  $l$ , integrating the flow vector by the shared surface between element  $l$  and  $m$ , see figure (2.2). Since the "no stress" criteria, i.e no compaction, has been applied for the groundwater system, the integral and derivative terms can be interchanged (2.26). No change in the volume of domain has been assumed. Approximating the time derivative with the first order finite difference, the numerical characterization has been distributed within the entire domain.

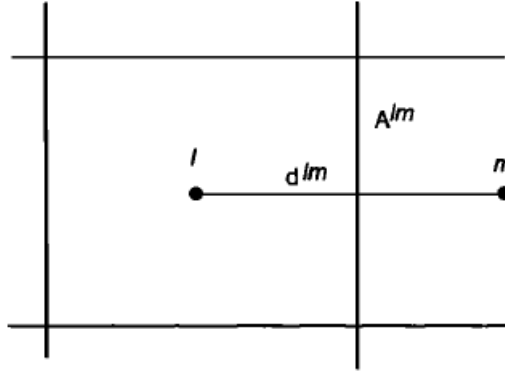


Figure 2.2. Center-to-center distance and interface between grid block I and its neighbor m.

Moreover, the simulator calculate the mass conservation for each time step,

## 2.4. NUMERICAL PARADIGM

---

and thus the negative value for the mole fraction of each element has reset to zero value then continues the iteration to reach to the convergence solution [1].

It is of importance to mention that the simulator applies upstream weighting for computation of the interface parameters. In other words, the value for the parameters has chosen based on the flow direction, parallel to the hydraulic gradient. In fact, the upstream weighting is to avoid convergence of the problem to nonphysical solutions [4]. For instance, in the water phase the upstream weighting is defined as:

$$\left(\frac{k_{rw}}{\mu_w}\right)^{lm} = (k_{rw}/\mu_w)^l \quad (2.27)$$

Simply means that the simulator presumes the upstream mobility value for the calculation in the given time interval.

The mass balance of component  $i$  has been elaborated for a discretized system, as well as the energy equation. However, for the isothermal system, the energy balance will be omitted, thus it is expected to have less computation time and more available memory [6].

### 2.4.2 Primary variable and Variable substitution

Due to the *Gibb's Law* the degree of freedom for the system with  $N$  component is  $F = N + 2 - NPH$ . However, the equation has been considered only for intensive properties[1]. Therefore, the latter information to determine the relative amount of each phase has been obtained from the saturation values which  $NPH - 1$  of these saturations are independent. The total number of freedom for the system turns to be  $F' = N + 2 - NPH + NPH - 1 = N + 1$ . As it is demonstrated by the equation, the degree of freedom of the system is independent of the number of existing phases.

The  $N + 1$  value is chosen as the primary variables, and based on number of existing phases within the grid block the unknown parameters is calculated. Note that the choice of the primary variable is not arbitrary and the number of phases in the grid block determines the set of variables to be chosen as primary variables [1].

### 2.4.3 Two and Three-Phase Capillary Pressures

Since in the multi phase system which is considered, i.e NAPL spill, the oil saturation is low, thus the capillary pressure would be low as well and can be neglected. But when it comes to the drying of the two or three-phase system, the capillary pressure will be fixed in the value corresponding to the irreducible liquid saturation.

The assumption is in a good agreement regardless of pressure gradient. Even though the liquid will be immobile in its irreducible saturation, the liquid droplets can evaporate [1].

### 2.4.4 Newton-Raphson Iteration

Generally, the system defined with the equation (2.26) has been solved by the iteration process. TMVOC uses the concept of the residual-based Newton-Raphson technique. Practically, the residual term refers to the amount in which the equation (2.26) fails to conserve the mass and energy defined for each chemical compound and thermal energy in each grid block [1]. The system residual vector has been elaborated by the following equation:

$$R(X) = 0 \tag{2.28}$$

Where both  $R$  and  $X$  are respectively the residual vector and primary variable unknowns [1]; Taylor series expansion around the assumed solution  $X^k$  is elaborated.  $k$  presents the iteration level. The linearized matrix equation will be

$$\left[ \frac{\partial R(X)}{\partial X} \right]^k (X^{k+1} - X^k) = -R(X^k) \tag{2.29}$$

The equation includes a linear system of  $NE(N + 1)$  equations to be solved for each iteration. Note that  $NE$  represents the number of volume elements within the domain, and the term  $N + 1$  is the set of primary variables for each grid block.

The purpose has been to reach to a convergent solution as soon as the the normalized residual of the every component is smaller than the convergence value set for the iteration run. Consider that the residual value of the component has obtained dividing the residual value to the the component value in the grid block at the beginning of each time step[1]. In addition, the time

## 2.4. NUMERICAL PARADIGM

---

step size has been set manually following the target of simulation in order to observe time evolution of the phenomena occurring in the ground water system. But when the convergence reaches before the maximum number of iteration, the size of the next time step will be doubled. It is a justified control command to better observe the variation of system dynamic behavior. However, when the convergence fails to reach within the inserted maximum number of iteration, the simulator reduces the time step size [18].

### 2.4.5 Boundary and initial conditions

The 3D boundary conditions basically have two wide categories: Dirichlet and Neumann boundary condition. Needless to say, there is Cauchy criteria which combines the two major types of the boundary criteria [3]. It enables the system to introduce a leakage term for semi-confined aquifer bed. However, in this case study, the two basic types satisfy the need for simulating the steady state regime and hydro-static pressure within the domain [19]. Specifically, the "no flux" boundary condition has been introduced as a common Neumann boundary condition which presents a typical confining bed throughout the lateral boundaries of the system [7]. To introduce the Dirichlet constant head boundary, the software provides the feasibility to keep the thermodynamic condition fixed for the boundary grid block, i.e fixed state cell. However, introducing a significant volume for the boundary cells is recommended to ascertain the constant thermodynamic parameters of the grid block [19]. Assuming inactive grid block is equal to excluding mass and energy balance for that cell, hence no unknown primary variable is included in the solution equation.

However, the primary values of the inactive grid blocks, i.e fixed state cell, has been used to calculate the flux term for the active adjacent cells within the domain [1].

Furthermore, the initial condition simply means the assignment of  $N + 1$  primary variables to the meshed system. It is accomplished by defining the number of phase. Afterwards, the saturation values and thermodynamic state has been employed.

### 2.4.6 Appearance and Disappearance of Phases

The software recognizes the appearing and disappearing of a phase with checking the thermodynamic compatibility for each grid block, by means of calculating the primary variables after each iteration level.

Note that the appearing of a phase is much of effort to recognize, likewise applying new state for the grid blocks. The software includes the probable present of NAPL criterion to check the all mole fraction using the equilibrium constants and mole fraction of the components. Applying the "would be" NAPL criteria, the software is able to robust the performance of simulation. Mathematically speaking, the criteria

$$\sum_i x_{iw}/K_{iwo} \geq 1 \quad (2.30)$$

is applied to check the evolution of the NAPL phase within the block that only was comprised of single phase [1].

Another problematic scenario is the re-initialization of the primary variables, which is essential to be addressed.

For instance, after the phase evolution of a given component into a grid block, i.e NAPL spill, the primary variables could be drastically different. Therefore, it is an absolute required to properly examine and check the validation of primary variables for the next iteration level. To do so, the similar concept of flash calculation has been adopted to enhance the computation speed and decrease the discrepancy of the simulation. A flash calculation involves simultaneous solution of the material balance as well as the phase equilibrium relations [1]. As a result, the composition of each thermodynamically stable phase and the overall mole fractions are calculated with the Newton-Raphson method [1].

# Chapter 3

## Modelling approach

Taking into account the mathematical equations that have detailed in the previous chapter, DNAPL spill in saturated zone has been modelled. The spill problem is comprise of two run segments for the purpose of the sensitivity analysis [19]. As first segment, the steady state condition is installed in the model domain. It has included hydrogeological and stratigraphical parameters to adjust a given water flow parallel to the aquifer bed in a cubic standard model. Then, the NAPL spill is introduced to the system to complete the spill scenario. In this phase, a single cell injection of the desired pollution is applied with constant mass rate. Afterwards, the effects of several hydrogeological and anthropogenic parameters on the spatio-temporal distribution of the NAPL is investigated. For the quantitative analysis of the results, the contaminated volume of the aquifer either by dissolved phase or DNAPL free phase are obtained by data extraction procedure. In fact, the output data of the spill scenario is undergone a data processing approach running Python code. It is recommended to refer to the code script inserted in the annex (A). The aim of the study was assessment of the software's capability to incorporate the influence of the examined parameters. The detail of the scenarios has been elaborated in section (3.3).

Beside that, two more run segments have been accomplished for the reference scenarios, regarding the redistribution of the NAPL spill with monitoring time of one year and subsequent pumping out of the contaminated volume of the aquifer. Relevant data is achieved to evaluate the removal efficiency of the applied remediation technology, i.e Pump and Treat facilities.

For the purpose of the modelling, Petrasim software has run TOUGH2 code which is developed at Lawrence Berkeley National Laboratory, Berkeley [18].

### 3.1. METHODOLOGY

---

The Graphical User Interface (GUI) of the software has provided a user friendly environment to facilitate the control on the parameters inserted by the Modeler. The adaptability of the software for simulation of NAPL spill and afterward pumping design have been demonstrated through the simulation outcomes.

## 3.1 Methodology

First of all, TMVOC simulator with relevant equation of states (EOS) have been assigned to initiate the model. Then, the primary set of variables has been assumed to hydraulically characterize the system, i.e hydraulic conductivity and porosity. To embed the multiphase flow within the domain while spill occurs, the controlling parameters of the spreading behavior such as capillary pressure ( $P_c$ ) and relative permeability ( $K_r$ ) of the phases have been extracted from the previous lab studies [22, 16]. The physico-chemical features of the volatile compounds have been already registered in the data base of Petrasim. The isothermal condition is applied to exclude the heat transfer phenomena. It is presumed that the amount of spill introduced to the domain is not enough to change the temperature profile in the aquifer. Note that polygonal meshing is chosen for the discretization of the model domain, see figure (3.2). The aim of polygonal meshing was the ability to introduce refinement area around the wellbore. It can be helpful tool when it comes to performing remediation plan by pumping operation. Furthermore, the refinement of the bottom cells is applied, in order to capture the NAPL pool with higher resolution. Desired boundary conditions have been applied to install the aquifer flow regime. For the reference scenarios, the aquifer bottom shape is extracted from the Sketch up stratigraphical tools, see figure (3.1). Moreover, as the last simulation phase pump and treat field design is implemented to capture the NAPL pools and to reduce the dissolve phase concentration in the aquifer.

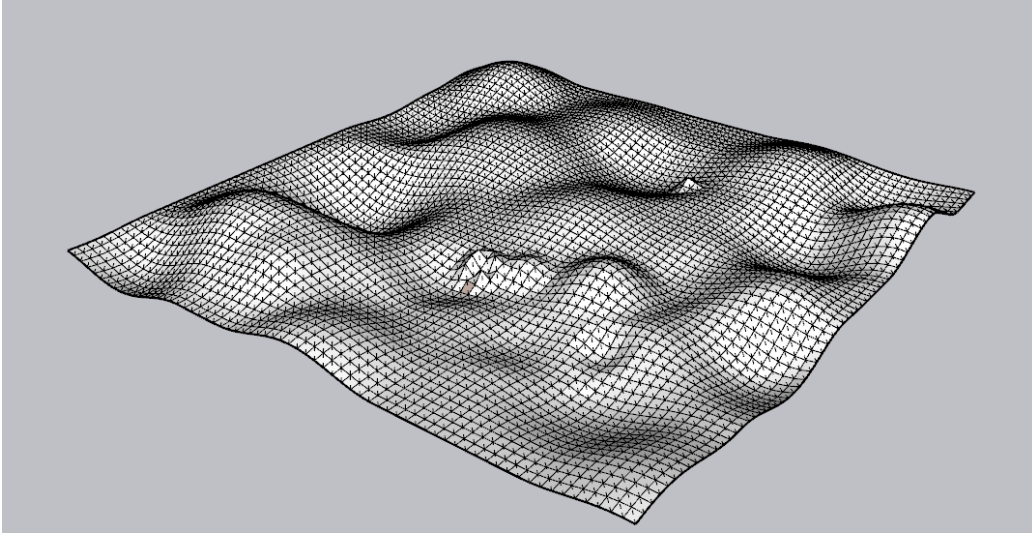


Figure 3.1. Sketch up design

#### 3.1.1 Initialization and Boundary Condition

The size of the model is assumed ( $100m \times 100m \times 5m$ ) in the 3-D Cartesian coordinates, see fig (3.2). For the Z-division, the custom meshing has been applied with more refinement cells in the last 2 meters of the layer [2]. The initial condition of  $P = 5$  bar and  $T = 14^\circ\text{C}$  have been set [18].

Furthermore, the linear pressure function has been assumed along the X and Z-axis to perfectly distribute the pressure values within the domain. Hence, the hydrostatic pressure along the layer is applied and different head value is assigned for initialization of the steady state flow condition horizontally to the confining bed. Needless to say, all the primary data set is provided by the literature to mimic the natural environmental groundwater flow [3, 7]. Note that different hydraulic gradient has been applied to study the effect of different water velocity into the spill dynamic. The detail is explained in the Section 3.3.

The two basic types of boundary condition have been applied to appropriately describe the energy and heat transfer close to the boundaries of the domain. Constant Head Boundary (CHB), i.e Dirichlet boundary condition, is introduced to the right and left lateral boundaries, shown arrows in Figure (3.2). The criteria is to sustain the pressure values in lateral boundaries and to install a steady-state flow condition. The specific "no flow" Neumann

### 3.1. METHODOLOGY

---

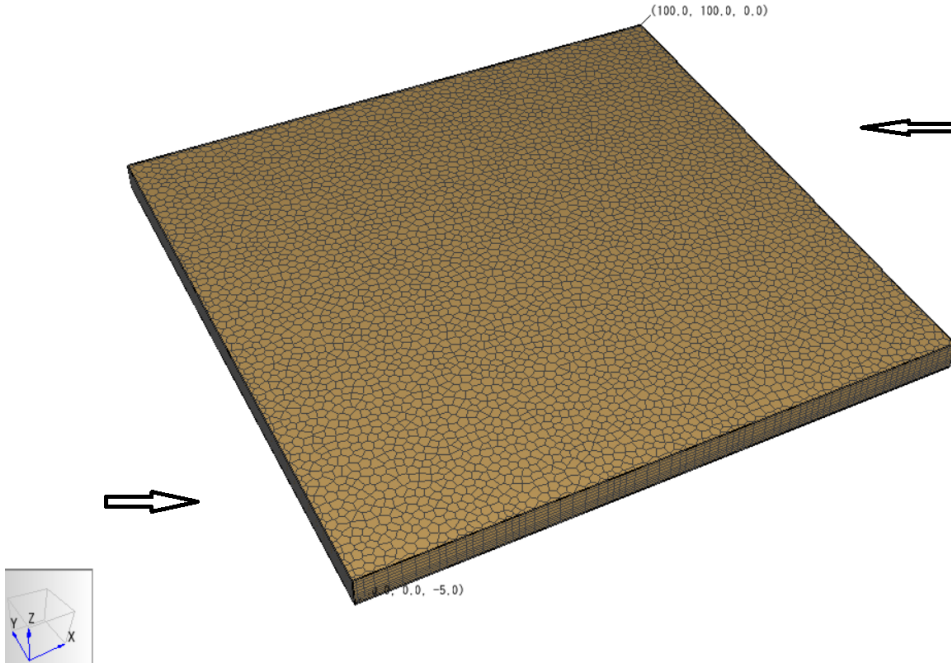


Figure 3.2. Standard 3-D model

boundary condition is also applied to the upper, bottom and the other lateral boundaries to represent the confining aquifer.

#### 3.1.2 Lithology and Mesh Gridding

The lithology of the sub-domain region is controlled by hydrogeological parameters including porosity, density of the rock, permeability tensor and specific heat capacity. The hydrogeological properties has been provided in a sense that it would be in a good agreement with Sandy Shallow aquifer. The hydraulic conductivity of  $K=2.34 \times 10^{-5}$ m/sec has been employed. The effective porosity of 0.24 is assigned with a matrix density of  $2600 \text{ kg/m}^3$ . The permeability value of  $k_{xy} = 2360 \text{ mD}$  has been assumed in the X-Y Plane, but the vertical permeability is  $k_z = 40 \text{ mD}$  to contribute to the horizontal flow along the bed, i.e. *Dupuit-Forchheimer (D-F)* approximation [3]. Note that the software supports either uniform rectangular (Prismatic) 3D grid or non-uniform polygonal (Voronoi) meshes. However, the polygonal mesh gridding has been considered as preferable tool to describe the flow behavior

### 3.2. RUN SEGMENTS

---

around the wells, due to the flexibility of refinement of the well bore area [18, 2]. Indeed, the polygonal meshing provides more control on the space and time evolution of the phenomena occurring in the ground water dynamic system [3]. The cell area is set to  $1.65\text{m}^2$ , with the maximum refinement area of  $0.2\text{ m}^2$  around near the well . In fact, it is chosen one order of magnitude less, in order to observe the wellbore area with higher resolution . After all, for the space discretization of the medium, i.e totally 49880 cells have been introduced by the polygonal meshing.

## 3.2 Run Segments

The simulation series that have been run for the Sensitivity analysis includes primarily, installing the hydrostatic pressure and the steady state flow condition within the domain. The second run segment is to introduce a source term of NAPL spill below the water table. As it is discussed before, two more run segment including monitoring of the NAPL redistribution in the aquifer for the period of one year and Pumping operation for the period of six month has been applied for the reference scenarios. Therefore, the procedure is detailed in the next sections.

### 3.2.1 Steady State Flow Condition

During the first phase, the constant hydraulic head difference has been applied to the lateral boundaries of the domain in order to install laminar flow horizontal to the confining bed, shown in Fig (3.3). "no flow" boundary condition is introduced to the other faces of the domain, assuming a confined aquifer [3, 7]. Notice that the hydraulic difference has been adjusted in a way to provide natural Darcy flow in the groundwater system,  $q = 0.1 - 1\text{ m/day}$  .

At initialization step, the system is comprised of one single fluid, i.e water, within the domain. Thus, the multi phase flow criteria is not required to be introduced in this phase. After the first run, it is expected to see the isopotential lines of which the flow lines are perpendicular. The simulation has been run successfully and the laminar flow lines has been produced almost horizontal to the confining bed, see figure (3.3).

### 3.2. RUN SEGMENTS

---

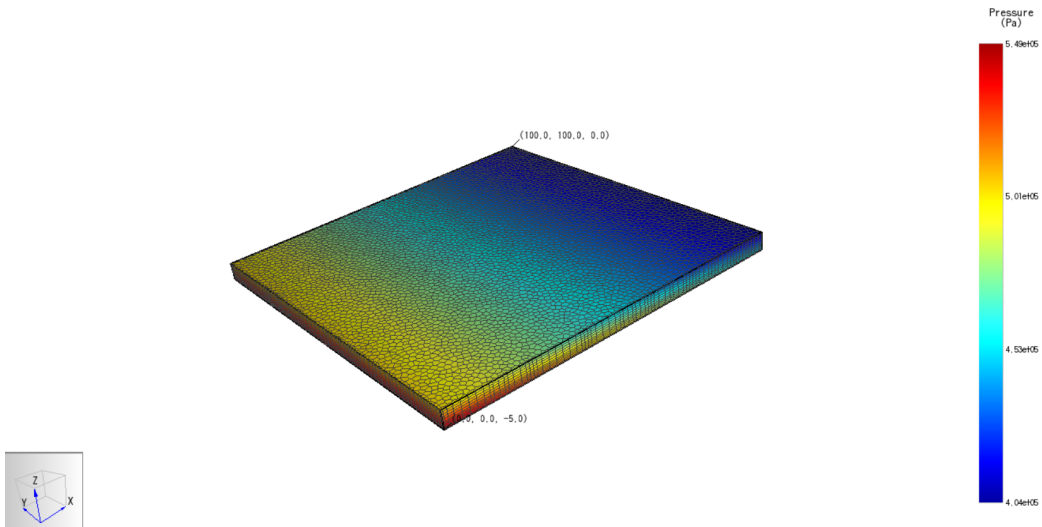


Figure 3.3. Steady state and hydrostatic pressure within the domain

#### 3.2.2 NAPL Spill

After reaching to the steady state condition within the domain, the new model has loaded the initial thermodynamic conditions from the previous simulation run [19]. For the spill scenario, monthly and yearly spill of 10 tons has been implemented. Moreover, two typical type of chlorinated solvent has been examined for the purpose of the modelling, i.e. TCE and PCE. The procedure is accomplished by single cell injection as a source term adjusting a constant mass rate and appropriate enthalpy value for substance.

Note that the heat transfer equation has been excluded during the simulation. Additionally, the multi phase flow controlling parameters, i.e relative permeability and capillary pressure, have been inserted, comprise of different models. In this case study, *Stone's Model* and *Parker's Three Phase* are applied respectively to the relative permeability and capillary pressure between the phases [7, 18]. Additionally the scaling parameters of the  $(P_c - S)$  and  $(K_r - S)$  has been reported in table [7].

### 3.2. RUN SEGMENTS

---

Table 3.1. Determined parameters for capillary pressure and relative permeability

	$P_c - S$ (Parker and Lenhard)	$K_r - S$ (Stone)
$S_{wr}$	-	0.1
$S_{nr}$	-	0.1
$S_{gr}$	-	0.0
$n$	2.5	2.5
$S_m$	0.1	-
$\alpha_{gn}$	100	-
$\alpha_{nw}$	50	-

The parameter's relationship with the phase saturation has been formulated to adjust the scaling factors ( $\alpha$ ), see table (3.1). In fact, the values have been opted in a way that the system properly models the DNAPL spreading behavior [7].

The seepage time for spreading the NAPL has been assumed one month and one year. The result of the simulation has shown graphically by means of cell oil saturation around the spill source.

#### 3.2.3 Monitoring NAPL Spread

Once the spill incident occurs, the monitoring is a crucial step to forecast the spill distribution within the aquifer. Therefore, the duration of one year has been assumed as monitoring time. The time and space evolution of the spill within the medium represents the mathematical formulation compatibility with the real system behavior. Therefore, the time steps has been chosen small enough to capture the phenomena taking place within the domain. Note that the initial thermodynamic condition has been loaded from the previous simulation run, i.e spill incident.

Hypothetically, the spill monitoring is carried out by means of better understanding the hydrogeological configuration and fluid flow effects on the spill dynamic behavior. Moreover, the expansion of the NAPL pool can be another parameter to be evaluated. The downward movement of the DNAPL confirms the gravity-density segregation of the NAPL phase. Meanwhile, the flow velocity continuously pushes the non aqueous phase forward unlike the high mobility contrast ratio, i.e ( $\frac{k_{ro}/\mu_o}{k_{rw}/\mu_w}$ ), which is higher than one. Beside that, the fingering phenomena is less probable to occur.

#### 3.2.4 Pump and Treat Design

The next step after monitoring is the field design of pumping facilities as a primary remediation technique. Basically, the aim of remediation is to extract the dissolved phase as well as NAPL phase to treat the water which is contaminated. Therefore, the prevision of the NAPL pool position and migration pathway of the dissolved phase are required to be addressed [9]. Beside that, the quantity of the pore volume which is contaminated provides practical information for optimization of the P&T apparatus.

### 3.3 Sensitivity Analysis

In this section, the sensitivity of the hydrogeological and anthropogenic parameters in the contaminant spatio-temporal distribution has been studied. Indeed, the previous works have targeted the NAPL infiltration process by the influence of the groundwater flow [7].

Correspondingly, the most probable scenarios to be targeted has been assumed: **oscillation of groundwater velocity, spill time, and different chlorinated solvents.**

#### 3.3.1 Examined Parameters

First of all, several parameters have been introduced to describe the spill evolution phenomena, then the quantification of the parameters took place by direct measurement through the software outputs:

1. **Groundwater velocity.** The previous studies has shown noticeable influence of groundwater velocities on dynamic spreading of the spill in the aquifer. Respectively, three different flow velocities of water ( $v_{water} = 0.08$  m/day ,  $0.43$  m/day,  $0.9$  m/day ) are applied by inducing different hydraulic gradient. The key parameters to be measured are:
  - (a) Offset point displacement (OD). In the case of no flow, the point which can hit the center of pool in the bottom of the aquifer is assumed as offset point.
  - (b) Area Of Influence (AOI). The maximum area that is contaminated by dissolved phase, following the Italian law [8]. The con-

### 3.3. SENSITIVITY ANALYSIS

---

centration isosurfaces that exceeds the threshold concentration, following Italian's law.

- (c) Maximum Saturation Zone ( $S_{max}$ ). The area of max NAPL saturation zone is of importance when it comes to approximate the NAPL contaminated volume.
  - (d) Inclination of the percolation path. The angle which it is measured by the deviation from the vertical offset axis. Obviously, that is affected by the transport capacity of the groundwater flow due to its viscous flow.
  - (e) Pool Length (PL). The elongation of the pool in the bottom of the aquifer has been studied due to the effect of ground flow hydraulics.
2. **Spill time.** The spill scenarios has been considered by application of two different injection rate. For this case, the spill of 10tons has been injected in the span of one month and one year. Therefore, the spill injection rate are respectively assumed 3.8gr/s and 0.32gr/s.
- (a) Permeation Pressure ( $P_{permeation}$ ). The pressure in which the system overcomes the formation pressure and reaches to a plateau trend with time evolution.
  - (b) Max Saturation Zone ( $S_{max}$ ). The maximum area of influence that the spill could be spread in the domain via monthly or yearly injection.
  - (c) Area Of Influence (AOI).
3. **TCE/PCE.** Implementing different chemical compounds to observe the spatio-temporal distribution of the plume within the domain, see table (3.2).

Table 3.2. Physico-chemical properties of TCE and PCE

Property	TCE	PCE
Chemical formula	$C_2HCl_3$	$C_2Cl_4$
Molecular weight (g/mol)	131.4	165.8
Density (kg/m <sup>3</sup> )	1462.0	1620.0
Viscosity(cP)	0.54	0.89
Vapor pressure (kPa)	2.5	9.2
Water solubility(molar frac)	$1.5 \times 10^{-4}$	$2.18 \times 10^{-5}$

### 3.3. SENSITIVITY ANALYSIS

---

- (a) AOI. The maximum area contaminated by the NAPL
- (b) Expansion factor (EF). The ratio between the expansion in X-axis (longitudinal) to Y-axis (lateral) has been investigated.
- (c) Sedimentation Time. The time in which the spill reach the bottom of the aquifer.
- (d) Off-Set Displacement (OD).

#### 3.3.2 Scenarios

For each flow velocity, different injection rate and spill component has been applied. Basically, NAPL spill problem is run for twelve scenarios. The dynamic evolution of the spill has been captured at given time intervals to compare the cases.

Schematically, for each scenario, the evolution of the dissolve phase is displayed through X-Z and X-Y cross sections of the aquifer system. Meanwhile, the migration path of the NAPL free phase is illustrated through X-Z slice of the domain.

To visualize the dissolved phase data and the NAPL saturation, the output data has undergone through a data processing approach, see annex (A). the aim was to quantify the high saturation area of the NAPL free phase ( $S_{max}$ ) and the area of influence(AOI) of the dissolved phase.

Following Italian's environmental law, the risk threshold concentration (CSC) of TCE and PCE are considered respectively  $1.5 \mu\text{g/L}$  and  $1.1 \mu\text{g/L}$ . The corresponding molar fractions has been obtained to extract the aquifer volume which has unacceptable concentration amount. The approach is to measure which portion of the cells obey the below criteria for TCE and PCE:

$$2 \times 10^{-10} \leq X_{TCE(aq)} \leq 1.51 \times 10^{-4} \quad (3.1)$$

$$1.19 \times 10^{-10} \leq X_{PCE(aq)} \leq 2.18 \times 10^{-5} \quad (3.2)$$

To address the NAPL phase , the same approach has been employed with the lower cut off ratio of  $S_{VOCs} = 0.001$ .

$$0.001 \leq S_{VOCs} \leq S_{Max} \quad (3.3)$$

It is speculated that the ratio of the high saturation zone to the pore volume can be representative of the probable NAPL pool volume in the aquifer.

### 3.3. SENSITIVITY ANALYSIS

---

Following the equation,

$$V_{norm} = \frac{V_{NAPL}}{V_{Porevolume}} \quad (3.4)$$

in which  $V_{NAPL}$  is obtained by applying the criteria (A.3). Beside, the positioning of the pool in the aquifer bed obviously has of same importance as its volume. Therefore, quantifying the relevant volume plus the graphical schematic of the NAPL phase in the aquifer, enables a cost effective approach for pump and treat design.

As it is discussed in section (3.3.1), further measurements have taken place for better describing the spill spreading behavior. Primarily, the inclination of the percolation path has been obtained from the angle between the offset axis of the spill and the first highest concentration cell on the aquifer bed. Keep in mind that the higher water velocity deviates the migration path. Therefore, it leads to longitudinal displacement of offset point, expecting higher inclination degree and offset displacement (OD). In fact, the transportation capacity of the water affects strongly the spill migration in the medium.

On the other hand, applying different seepage time simply is equal to change the injection rate. therefore, the initial injected mass confronts the formation pressure and then starts to permeate into the system. Thus, the difference in permeation pressure and the initial pressure of the injection cell is assumed to represent the spill intensity. However, the higher time seepage (low injection rate) would decrease the maximum saturation value of the NAPL phase, the contaminated area would significantly increase. Hence, the dissolved phase evolution will be another factor to keep in mind when it comes to reclamation of the polluted site.

As another parameter to be examined, TCE and PCE are introduced by single source cell injection. The pool expansion has been captured as Expansion Factor (EF) of NAPL pool within the medium, taking into account different chlorinated solvent. By that, the versatility and sensitivity of the system to the kinematic parameters of different VOCs component is examined. The graphical result is shown for each scenario, providing the evolution frame of the spill behaviour in the aquifer system. Presumably, the higher density and viscosity of the PCE brings the assertion of less expansion factor and less pool elongation. Conceptually, the water shear force is not able to properly displace the fluid, hence resulting in less plume generation. For the same reason, the accumulation term takes more time to disperse within the

### 3.3. SENSITIVITY ANALYSIS

---

aquifer system, expecting higher maximum saturation value in the PCE case. Furthermore, it is expected to see shorter sedimentation time for the PCE case as well, due to the higher density contrast to water.

The relevant figures demonstrate the cross sectional evolution of dissolved phase as well as the NAPL migration path under different flow velocities. The downward movement of the DNAPL is observed regardless of the applied different flow velocities. TCE spill of monthly and yearly with water velocity of  $v_{water} = 0.08$  m/day has been illustrated on fig (3.4). Qualitatively, higher area of influence (AOI) is captured for yearly spill unlike the low water flow velocity.

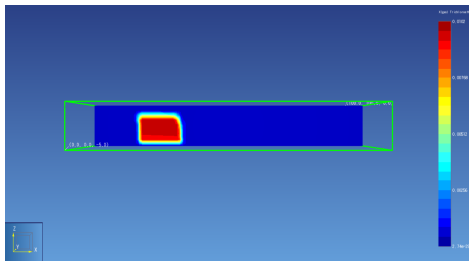
The same hydrogeological setup has been accomplished and illustrated for PCE, figure (3.7). As it is shown, the dynamic behaviour of the system evolves similarly as in the TCE case. Theoretically, the higher water flow velocity, the higher inclination and longer sedimentation time are expected. Considering different hydraulic gradients, two other flow velocities of  $v = 0.43$  m/day and  $v = 0.9$  m/day have been employed for TCE, see figure (3.5) and figure (3.6). Likewise, the peer scenarios have run for PCE as another spill component, see figure (3.8) and figure (3.9). It is observed that the higher induced flow velocity results in significant enlargement of the created pool either in monthly or yearly spill.

It should not be overlooked that the evolution of the dissolved phase is strictly twisted to the hydraulic potential of the underground water system. In real cases, pumping of the drinking water induces preferential flow pathways which can facilitated the faster dispersion of the dissolved phase. Qualitatively, the similarity between physico-chemical properties of TCE and PCE has resulted in the same dynamic spreading pattern. However, due to the higher density and viscosity of PCE, higher expansion factor is reported with the data interpretation.

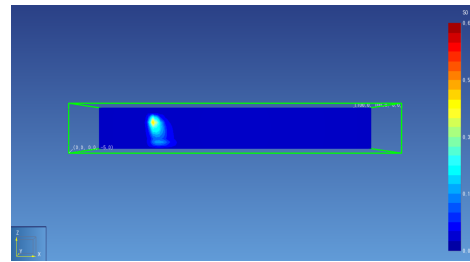
However, it is clear that the longer spill time concludes in larger contaminated area unlike introducing the same amount of spill. The quantitative outcomes of the scenarios are reported in the result section, see section (3.3.3).

### 3.3. SENSITIVITY ANALYSIS

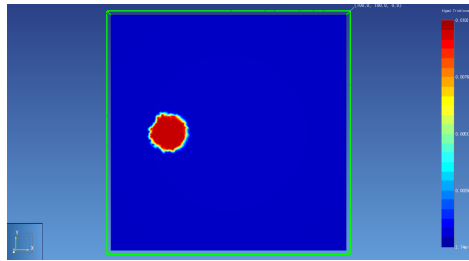
---



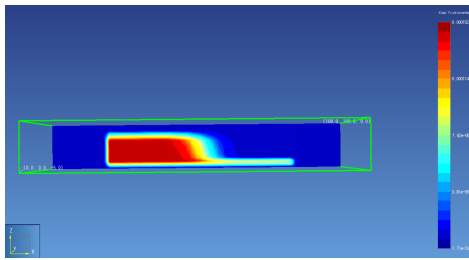
a: Monthly dissolved phase, X-Z



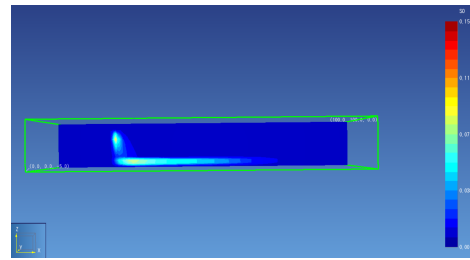
b: Monthly NAPL free phase, X-Z



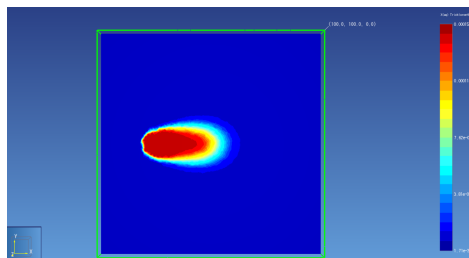
c: Monthly dissolved phase, X-Y



d: Yearly Dissolved phase, X-Z



e: Yearly NAPL free phase, X-Z

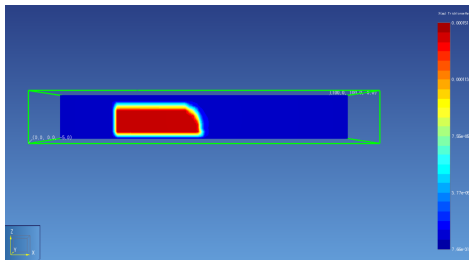


f: Yearly dissolved phase, X-Y

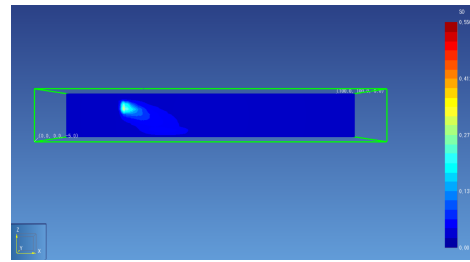
Figure 3.4. TCE spill. Slice view  $v_{water} = 0.08$  m/day

### 3.3. SENSITIVITY ANALYSIS

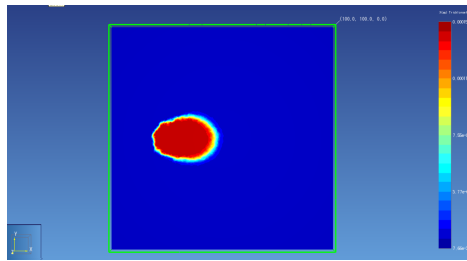
---



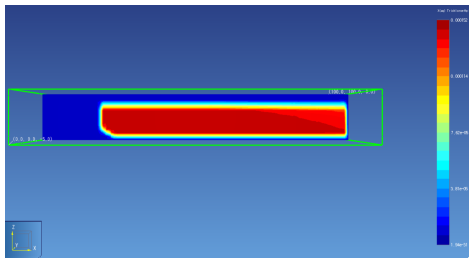
a: Monthly dissolved phase, X-Z



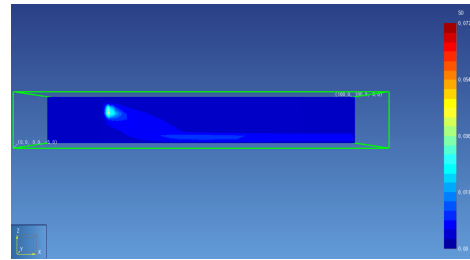
b: Monthly NAPL free phase, X-Z



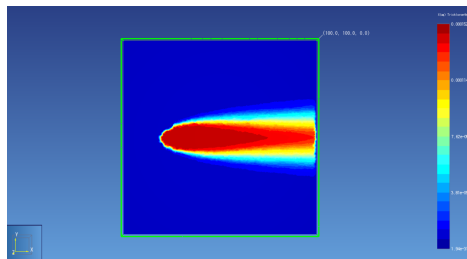
c: Monthly dissolved phase, X-Y



d: Yearly dissolved phase, X-Z



e: Yearly NAPL free phase, X-Z

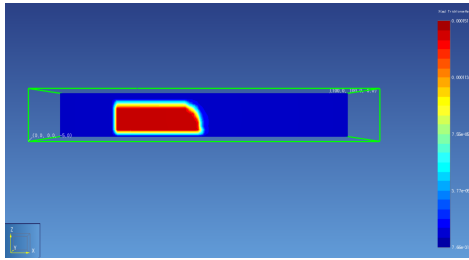


f: Yearly dissolved phase, X-Y

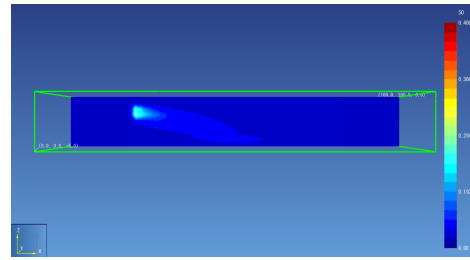
Figure 3.5. TCE spill. Slice view  $v_{water} = 0.43$  m/day

### 3.3. SENSITIVITY ANALYSIS

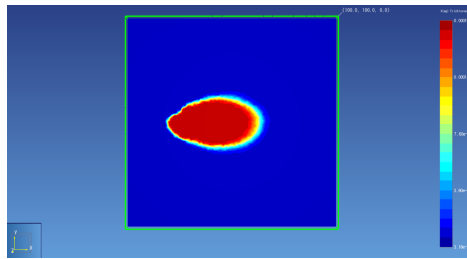
---



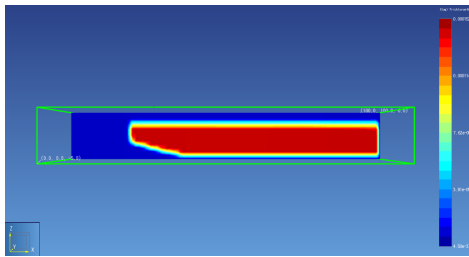
a: Monthly dissolved phase, X-Z



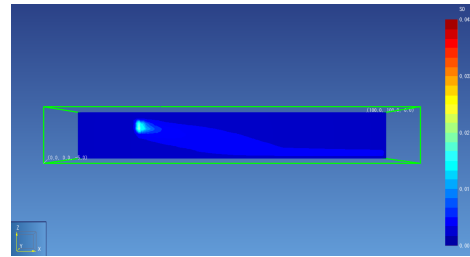
b: Monthly NAPL free phase, X-Y



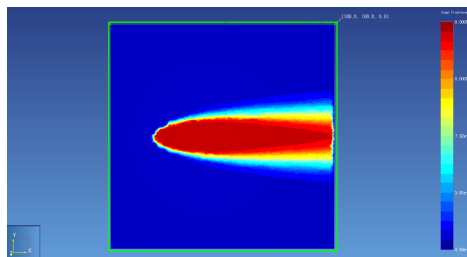
c: Monthly dissolved phase X-Y



d: Yearly dissolved phase, X-Z



e: Yearly NAPL free phase, X-Y

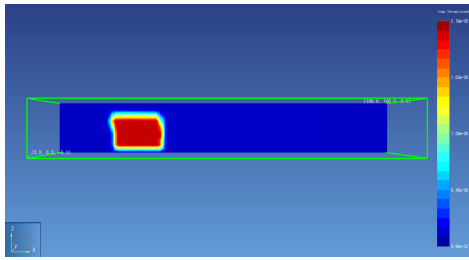


f: Yearly dissolved phase, X-Y

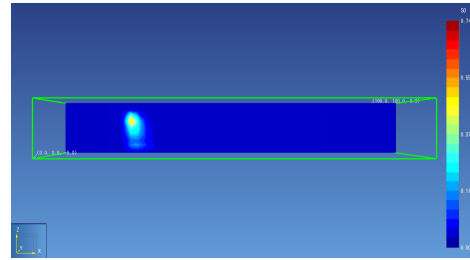
Figure 3.6. TCE yearly spill,  $v_{water} = 0.9$  m/day

### 3.3. SENSITIVITY ANALYSIS

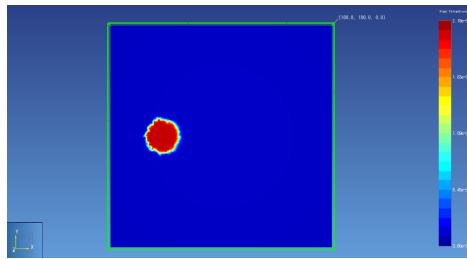
---



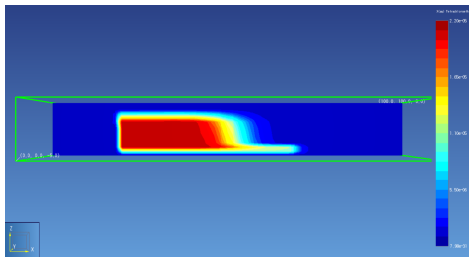
a: Monthly dissolved phase, X-Z



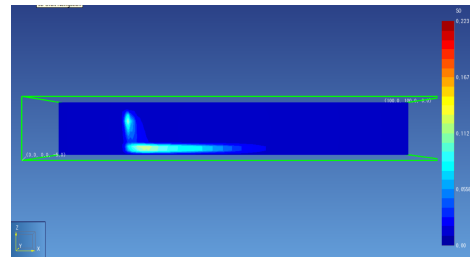
b: Monthly NAPL free phase, X-Y



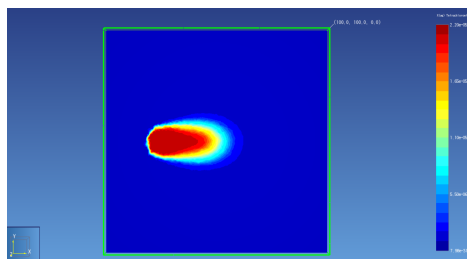
c: Monthly dissolved phase, X-Y



d: Yearly dissolved phase, X-Z



e: Yearly NAPL free phase, X-Y

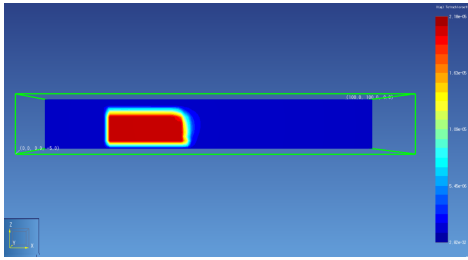


f: Yearly dissolved phase, X-Y

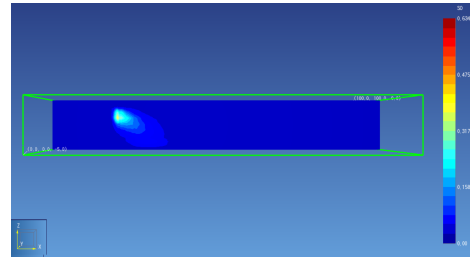
Figure 3.7. PCE spill. Slice view  $v_{water} = 0.08$  m/day

### 3.3. SENSITIVITY ANALYSIS

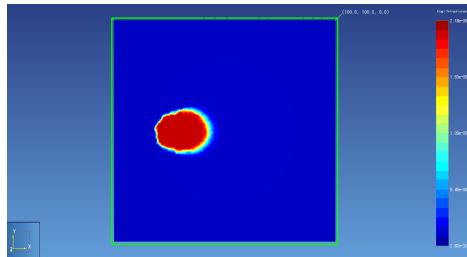
---



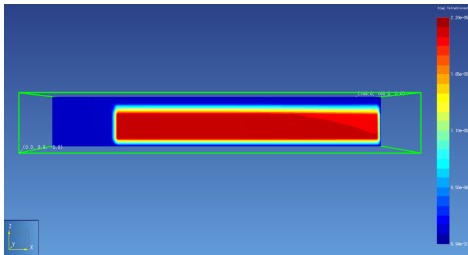
a: Monthly dissolved phase, X-Z



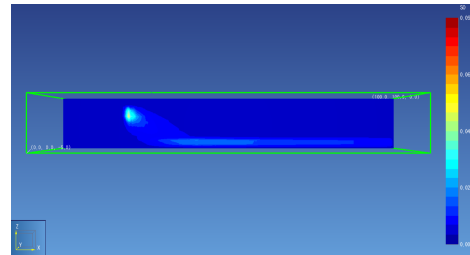
b: Monthly NAPL free phase, X-Y



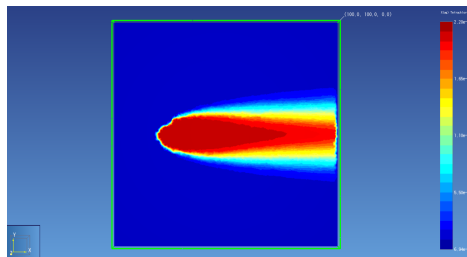
c: Monthly dissolved phase, X-Y



d: Yearly dissolved phase, X-Z



e: Yearly NAPL free phase, X-Y

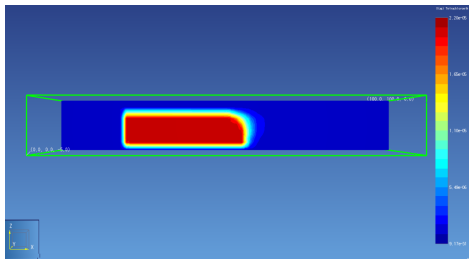


f: Yearly dissolved phase, X-Y

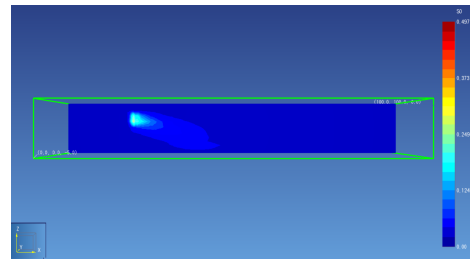
Figure 3.8. PCE spill. Slice view,  $v_{water} = 0.43$  m/day

### 3.3. SENSITIVITY ANALYSIS

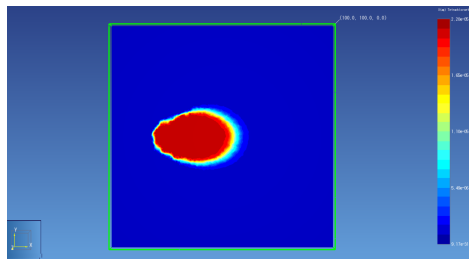
---



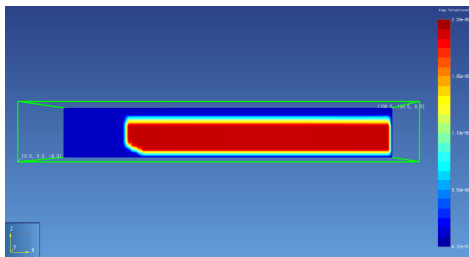
a: Monthly dissolved phase, X-Z



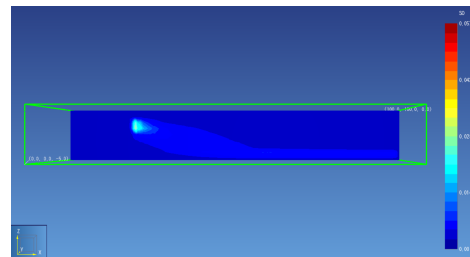
b: Monthly NAPL free phase, X-Y



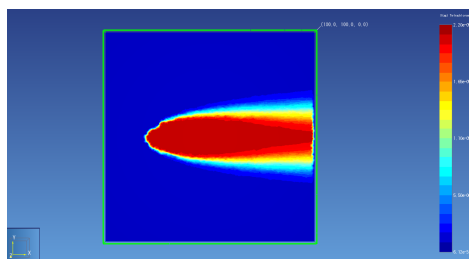
c: Monthly dissolved phase, X-Y



d: Yearly dissolved phase, X-Z



e: Yearly NAPL free phase, X-Y



f: Yearly dissolved phase, X-Y

Figure 3.9. PCE spill. Slice view,  $v_{water} = 0.9$  m/day

### 3.3. SENSITIVITY ANALYSIS

#### 3.3.3 Results

After the Simulation runs, the relevant data is acquired. The set of parameters has been collected respectively for monthly and yearly spill of both chlorinated contaminants under different flow velocities, see table (3.3) and (3.4).

As it was expected, the percolation deviation of the both contaminant has been significantly changed when the water flow velocity is enhanced, inclining to the flow direction. The reported data proposes that the inclination trend is similar regardless of different spill rate. Slight decrease in the percolation for the yearly spill (low injection rate) can be explained by the less resistance to the local flow regime. However, the higher viscosity and density of the PCE resulted in lower inclination than in the TCE case. Note that the percolation of the spill precedes the displacement of the off-set point, leading to generation of the NAPL pool farther than the spill point. Moreover, higher flow regime postpones the sedimentation of the NAPL phase, due to the transportation capacity of the groundwater flow. The higher inclination degree result in a longer migration path, thus contaminating larger area while moving down gradient. beside that, the quantification of the contaminated volume ( $V_{norm}$ ) would reveal the spatial distribution of the free NAPL phase.

Table 3.3. the impact of different flow velocities and different chlorinated solvents on monthly spill spread

	Groundwater flow velocity(m/day)					
	TCE case			PCE case		
	$v_{water} = 0.08$	$v_{water} = 0.43$	$v_{water} = 0.9$	$v_{water} = 0.08$	$v_{water} = 0.43$	$v_{water} = 0.9$
Percolation Inclination of the spill(°)	33.6	56.8	82	31	50.2	74.7
EF <sup>a</sup>	0.84	-	-	0.88	-	-
AOI ( $m^3$ )	285.12	699	1286.8	372.5	861.6	1555.2
$V_{norm}$	0.011	0.023	0.044	0.008	0.018	0.033
OD <sup>b</sup> (m)	2	-	-	1.3	-	-
Pool Length <sup>c</sup> (m)	11	-	-	9	-	-
Max. DNAPL saturation( $S_{Max}$ )	0.694	0.55	0.408	0.744	0.634	0.497
$t_{Sedimentation}$ (days)	14	> 30	> 30	11	20	27
$P_{Permeation} - P_{Initial}$ (Pa)	1038.7	1039	1034.7	973.4	977.3	974

a,b,c the data are obtained when there is generated pool.

The expansion factor (EF) of the NAPL pool controls the spreading pattern of the NAPL phase in the multiphase flow system. Practically, the mobility ratio of the contaminant determines the expansion factor of the spill. The higher mobility contrast between the phases leads to higher EF value. However, the higher water flow regime forces the spill into the longitudinal

### 3.3. SENSITIVITY ANALYSIS

extension, thus less expansion factor is reported.

Taking into account the capillary and mobility of the NAPL phase, the lateral expansion of the TCE is reported lower than PCE in all cases. It can be concluded that the expansion factor(EF) is higher in the PCE spill. Note that this contrast is more tangible when the injection rate is low, as it is reported in the table (3.3) and (3.4). It reveals that the low water velocity can not displace the NAPL phase properly. Therefore, it comes out that the higher EF, the wider is the generated NAPL. Basically, EF value close to one is expected for a bigger front of the free NAPL phase.

Table 3.4. The impact of different flow velocities and different chlorinated solvents on yearly spill spread

	Groundwater flow velocity(m/day)					
	TCE case			PCE case		
	$v_{water} = 0.08$	$v_{water} = 0.43$	$v_{water} = 0.9$	$v_{water} = 0.08$	$v_{water} = 0.43$	$v_{water} = 0.9$
Percolation Inclination of the spill( $^{\circ}$ )	29	50	81	23	43	79
EF	0.39 <sup>a</sup>	0.43 <sup>b</sup>	0.26 <sup>b</sup>	0.6 <sup>a</sup>	0.48 <sup>b</sup>	0.4 <sup>b</sup>
AOI ( $m^3$ )	495.1	2063.3 <sup>b</sup>	2862.5 <sup>b</sup>	553.7	2172 <sup>b</sup>	3398 <sup>b</sup>
$V_{norm}$	0.008	0.024 <sup>b</sup>	0.032 <sup>b</sup>	0.007	0.021 <sup>b</sup>	0.035 <sup>b</sup>
OD (m)	5.9 <sup>a</sup>	23.5 <sup>b</sup>	37.3 <sup>b</sup>	3.8 <sup>a</sup>	17 <sup>b</sup>	33.2 <sup>b</sup>
Pool Length (m)	52.2 <sup>a</sup>	37 <sup>b</sup>	46 <sup>b</sup>	41.2 <sup>a</sup>	33 <sup>b</sup>	44 <sup>b</sup>
Max. DNAPL saturation( $S_{Max}$ )	0.156	0.073	0.043	0.223	0.092	0.058
$t_{Sedimentation}(days)$	21	40	52	14	32	45
$P_{Permeation} - P_{Initial}(Pa)$	150.4	136	126	156.5	145.3	311

<sup>a</sup> the data are obtained at the end of spill time.

<sup>b</sup> the data are obtained at last captured pool within the domain,  $t_{seepage} = 3month$ .

The off set displacement (OD) of the spill varies in a wide range when the water flow is augmented. The displacement increases form 5.9 m to 37.3 m in the case of yearly TCE spill while the water flow has changed from  $v_{water} = 0.08$  m/day to  $v_{water} = 0.9$  m/day. It can be concluded that the flow velocity plays critical role in positioning of the NAPL pool. OD strictly follows the percolation trend. Referring to the collected data, OD of the PCE spill will be less than TCE spill. The reason largely is due to different kinematic parameters of the components. However, for the water velocities of  $v_{water} = 0.43$  m/day and  $v_{water} = 0.9$  m/day, no generated pool is reported for the monthly spill.

The elongation of the generated pool for the yearly spill is noticeable regardless of the lower maximum saturation of the NAPL phase. It is ascertained that the NAPL phase accounts for secondary source of the dissolved contaminant generation. Thus, containing the NAPL pool requires a great deal of

### 3.3. SENSITIVITY ANALYSIS

---

effort for optimized design of the pump and treat field. comparing the TCE and PCE, the length of the generated pool is relatively lower for PCE, even though the expansion factor of the PCE spill is correspondingly high. Therefore, the pool length should be taken into account with the expansion factor, in order to give dissertation about the dynamic evolution of the NAPL pool. Analyzing the maximum saturation value for different flow velocities, a drastic change is observed when the flow increases. The phenomena was expected due to the effect of higher advective flow which acts as a carrier agent. For instance, in the case of monthly spill of the TCE, the saturation value drops from 0.694 to 0.408 for one order of magnitude change in the flow velocity. Practically, the higher saturation zone is expected to be near the source sell area.

After all, the difference between the permeation pressure and initial pressure of the source cell is reported. Referring to the table (3.3) and (3.4), the value is almost constant for any flow velocity of the desire spill component. It shows that the pressure build up is independent of the flow velocity. However, the build up pressure requires to overcome the formation pressure and then dissipates within the medium. Comparing the value for different spill rate, the permeation pressure follows the same proportional of change with the injection rate. It is observed that the pressure variance for the PCE case is less than TCE, in the case of monthly spill. However, when it comes to the yearly spill the reported value is higher for the PCE case. It is suggested that the higher mass flux introduces a local turbulent regime, thus providing higher hydraulic gradient along the flow regime and shorter accumulation time is expected.

Considering different flow velocities for the monthly spill of TCE, AOI has reached from 285.12 m<sup>3</sup> to 1286.8 m<sup>3</sup> when water velocity is changed from  $v_{water} = 0.08$  m/day to  $v_{water} = 0.9$  m/day. In fact, the enlargement of the dissolved area is consequence of the higher advective flow rate. The data reported in figure (??) and figure (3.10) demonstrate the importance of water flow velocity in the spatio-temporal distribution of the dissolved phase under different injection rate.

AOI is obtained for different spill rate at the end of one month spill (monthly and yearly spill), figure (3.11). The result shows that PCE plume generation is enhanced by increasing the underground flow velocity, regardless of less solubility into water with respect to TCE. The reason would be the presence of large amount of the DNAPL phase in the contaminated aquifer, which equilibrates the chemical potential of the component in all the phases. Thus,

### 3.3. SENSITIVITY ANALYSIS

---

continuous generation of dissolved phase is expected. Once high flow velocity is applied the contrast between the AOI value is more noticeable. It can be speculated that the enlargement of the NAPL plume provides more contact with the water phase, thus generating excessive volume of the plume. Needless to say, the flow velocity has huge impact on the distribution of the dissolved phase within the aquifer system.

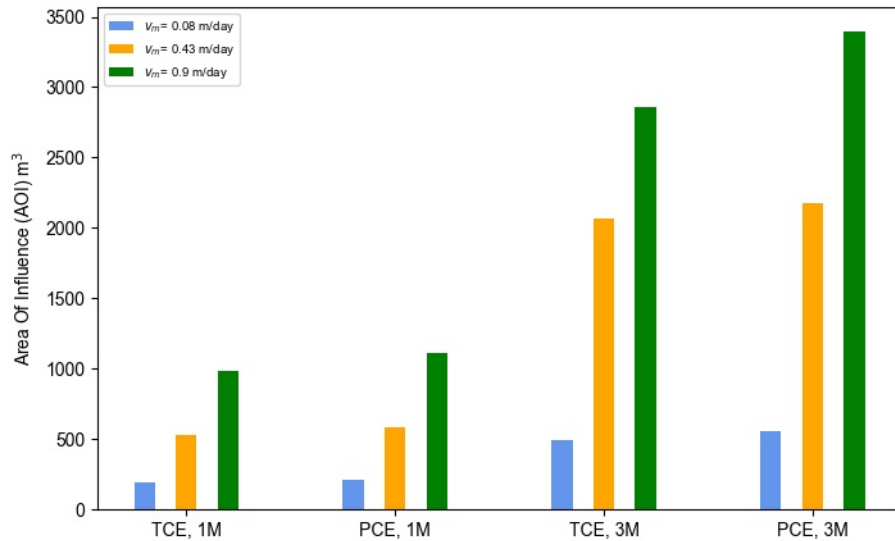


Figure 3.10. the spatial evolution of the Yearly spill captured for  $t_{seepage} = 1$  month and  $t_{seepage} = 3$  month

Beside that, the AOI value is monitored for the yearly spill at  $t_{seepage} = 1$  month and  $t_{seepage} = 3$  month. The proportional change in the contaminated volume of the dissolved phase is reported corresponding to different physicochemical properties of the contaminant, fig(3.10). Even though the yearly spill rate is relatively low, higher seepage time produces larger amount of dissolved phase. Consequently, the prevision of the contaminated volume by dissolved phase can be promising element to be taken into account when it comes to dimensions of the generated plume. Theoretically, higher pumping rate would be applied for enlargement of the cone depression around the well bore, in order to contain the contaminant plume. By that, the dissipation

### 3.3. SENSITIVITY ANALYSIS

---

of the dissolved phase is hindered with higher drawdown ( $s$ ), i.e change in the water level while pumping out the contaminated water. Note that the applied criteria for evaluation of the AOI is more conservative in the case of PCE, since it has higher toxicity index. Meanwhile, to reach to the target concentration, i.e. below CSC, the amount of volume which is required to be treated is key tool to perform ex-situ remediation, i.e Pump and Treat technique.

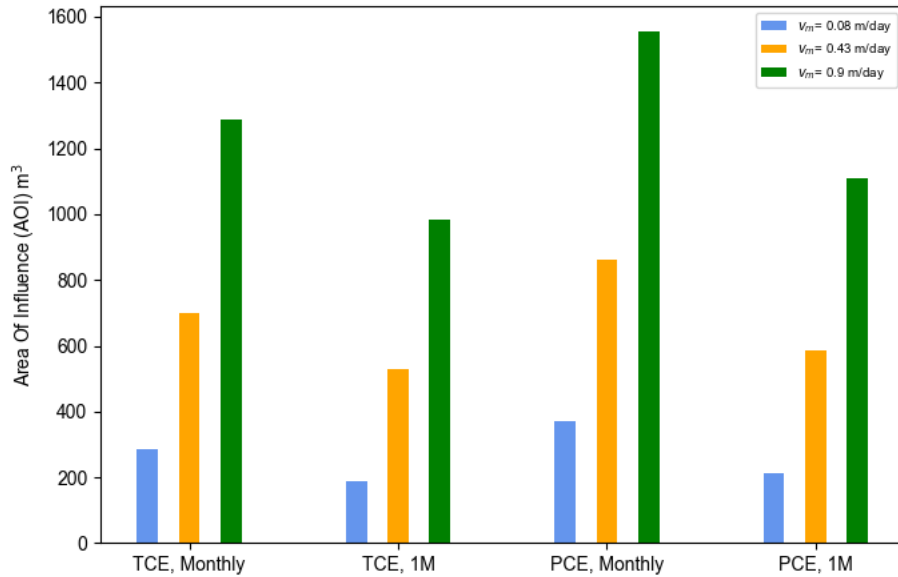


Figure 3.11. Area of influence for different injection rate

The saturation value of the grid data is collected to obtain the ratio of pore volume which represents the NAPL volume. Notice that  $V_{norm}$  is representative of the NAPL high saturation zone within the system.  $V_{norm}$  is obtained for monthly spill and yearly spill. For the yearly spill, since after three months the NAPL spill moves out of the domain, the spill evolution is reported for  $t_{seepage} = 1$  month and  $t_{seepage} = 3$ , see figure (3.12). Referring to the figure, in the case of monthly TCE spill, the occupied pore volume has increase 300% once the flow velocity reaches from  $v_{water} = 0.08$  m/day to  $v_{water} = 0.9$  m/day. However, the influence of higher advective flow rate significantly

### 3.3. SENSITIVITY ANALYSIS

increase the NAPL expansion in the aquifer, thus occupying larger portion of the aquifer volume. Considering TCE and PCE, the lower mobility ratio of the PCE results in less diffusion of the NAPL phase regardless of having higher diffusion coefficient. In fact, the enlargement of the NAPL phase correspondingly enhance the diffusion of the dissolve phase. On the other side, the extension of the NAPL contact area leads to excessive generation of NAPL plume.

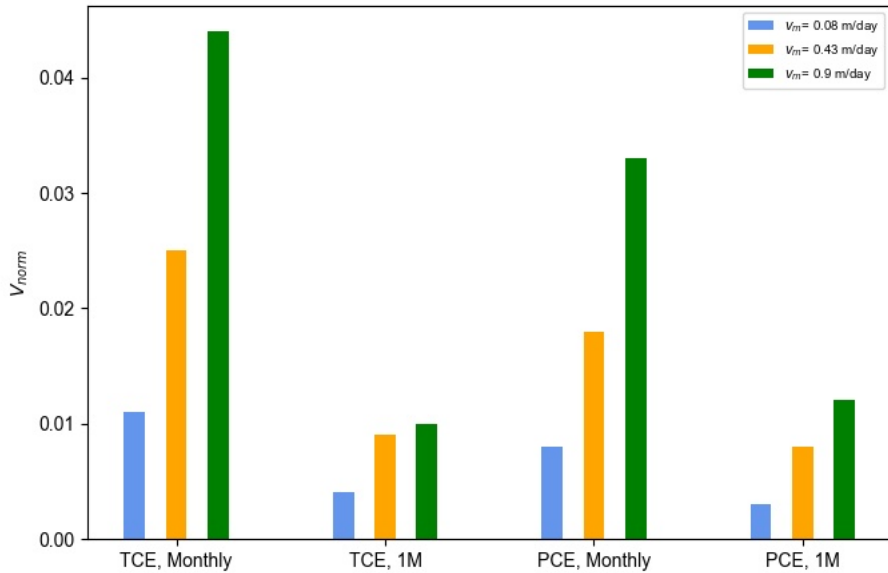


Figure 3.12. High saturation zone( $S_{max}$ ) for different injection rate captured at  $t_{seepage} = 1$  month

Furthermore, the impact of different injection rate is reported in figure (3.13) for time interval of  $t_{seepage} = 1$  month, comparing the monthly and yearly spill incident. At low injection rate(yearly spill), for  $v_{water} = 0.08$  m/day and  $v_{water} = 0.43$  m/day, the occupied volume of the TCE is bigger than the PCE case. However, at  $v_{water} = 0.9$  m/day, the value exceeds for the PCE case. the explanation of the phenomena is rooted in the hydraulic potential of the field. It can be claimed that the higher water flow regime has overcome

### 3.3. SENSITIVITY ANALYSIS

---

the kinematic difference of the chemical compounds.

Note that the flow velocity has inevitable effect on dynamic spreading of the spill. It is concluded that the injection rate as an anthropogenic parameter, can lead to different pattern of the NAPL phase distribution within the aquifer.

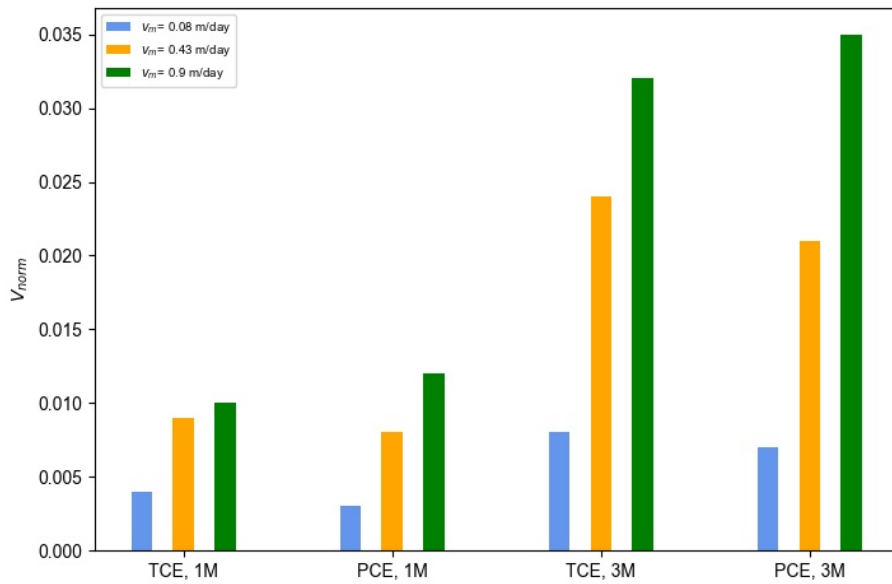


Figure 3.13. The NAPL phase normalized volume for the Yearly spill captured for  $t_{seepage} = 1$  month and  $t_{seepage} = 3$  months

For further analysis, the  $S_{max}$  reached within the system is plotted as function of time and shown for monthly and yearly spill of different VOCs, see figure (3.14) and (3.15). Hypothetically, the high saturation zone normally belongs to the injection source cell, since the injected mass initially accumulate in the source cell then dissipated due to advective diffusive flow governing the system. For the monthly case, the trend reaches to a plateau after a given time, see figure (3.14). As it is reported in the graph, the maximum saturation value PCE is relatively higher under each flow velocity, confirming the effect of kinematic parameter of the components. The trend follows the

### 3.3. SENSITIVITY ANALYSIS

---

same principle for the yearly spill of the contaminants. However, for the case of yearly spill, an anomaly has been observed when the water velocity is  $v_{water} = 0.08$  m/day.

Through the data analysis, it reveals that in the case of low water velocity and low injection rate, the high saturation zone migrates to the bottom of the aquifer. The phenomena is captured for both TCE and PCE case, see figure (3.15). Note that in the case of low water flow velocity the sedimentation time of the NAPL is shorter. In fact, the graph first had a ascending trend in which the high saturation belong to the source cell. then due to the shorter sedimentation time, the accumulation of the NAPL phase take place on the bottom of the aquifer. The second ascending trend demonstrates the transition of the high saturation zone within the domain. Therefore, comprehensive understanding of the coupled parameters is essential to predict the dynamic behavior of the spill.

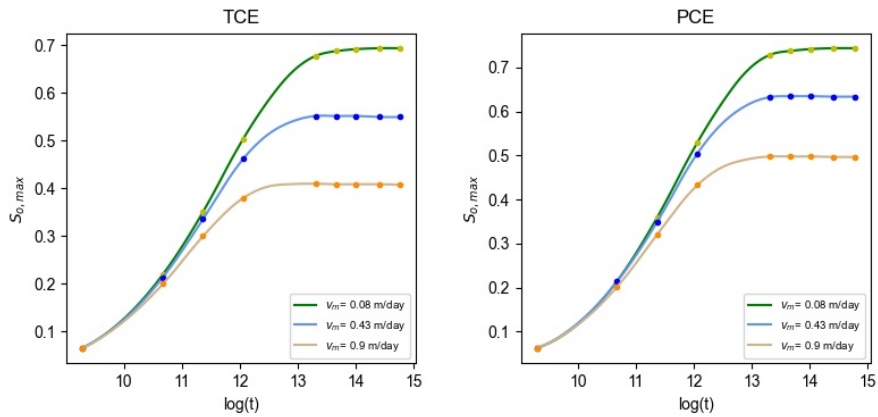


Figure 3.14. TCE and PCE Monthly spill,  $S_{max}$  vs  $\log(t)$

### 3.4. REFERENCE SCENARIOS

---

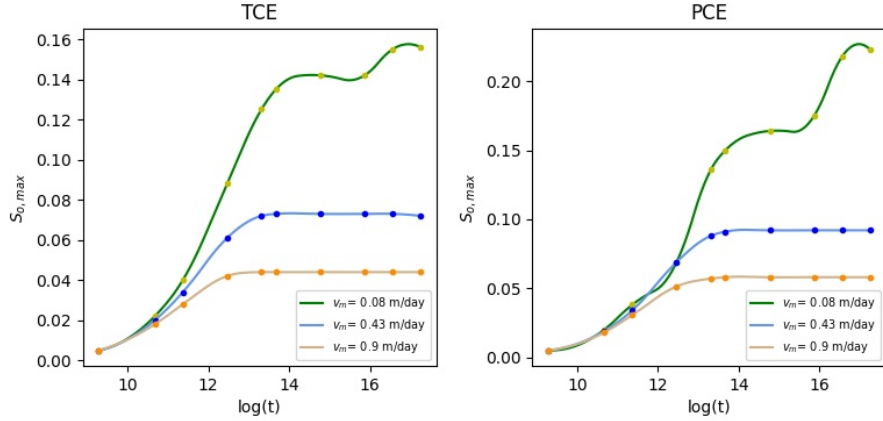


Figure 3.15. TCE and PCE yearly spill,  $S_{max}$  vs  $\log(t)$

## 3.4 Reference Scenarios

In the previous section, the sensitivity of the system dynamic behavior has been elaborated based on three different parameters. However, the previous studies has emphasized the importance of the bottom stratigraphy of the aquifer. Note that the DNAPL is quite likely to be trapped in the geological unconformities. It is clear that the trapped NAPL pool is a secondary source of the plume generation. Therefore, the bottom topography of the aquifer has been extracted by Sketch-up tool for building the stratigraphy layer, see figure (3.1).

Determining the possible isolated NAPL pool would contribute to the efficiency of the pump and treat design. For that reason, two possible incident scenarios have been developed with monitoring of one year. then, the pump and treat technique is applied with six month operation time to optimize the removal efficiency of the NAPL phase and to contain the plume generated by the spill.

### 3.4.1 Pipe Leakage

The release of 50 kg/day of TCE has been introduced by single cell injection to the aquifer system for a period of 200 days. Furthermore, the Pump and Treat facilities has been designed for the remediation of contaminated

### 3.4. REFERENCE SCENARIOS

---

area. Primarily, the ground water velocity of  $v_{water} = 0.43$  m/day is adjusted. Then, the steady state condition has been run for pressure and temperature distribution within the aquifer, see fig (3.16).

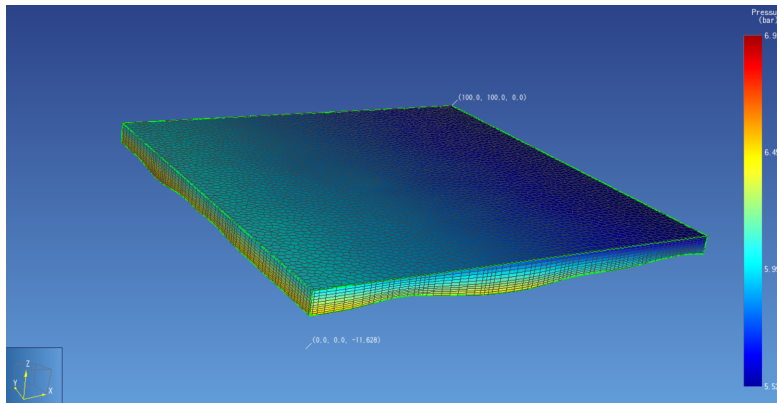
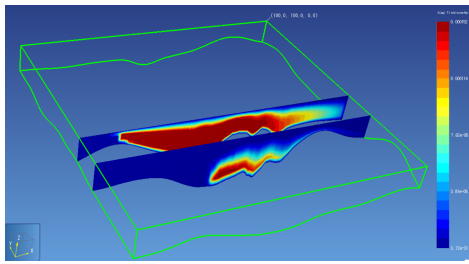


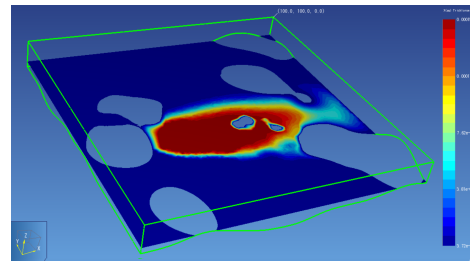
Figure 3.16. Hydrostatic pressure distribution in the system

The spill position is assumed close to the right boundary of the system, right below the water table. The positioning of the NAPL phase within the medium has been captured after monitoring of the system for period of one year. At the end of simulation time, the DNAPL phase has been detected in four spot, in which one of the NAPL pool is completely isolated. regardless the NAPL pool size, it is able to constantly introduce dissolved phase to the underground water system.

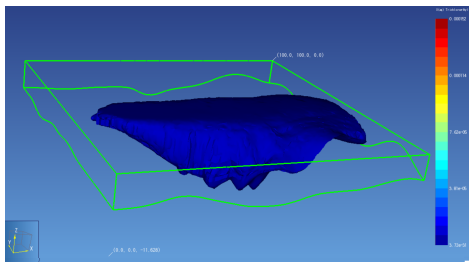
### 3.4. REFERENCE SCENARIOS



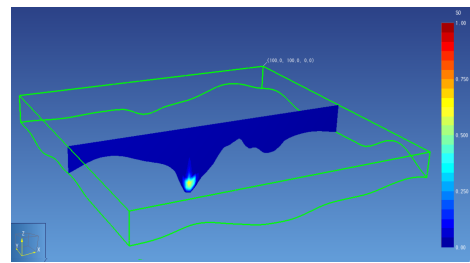
a: X-Z slice of the dissolved phase passing through the NAPL pools



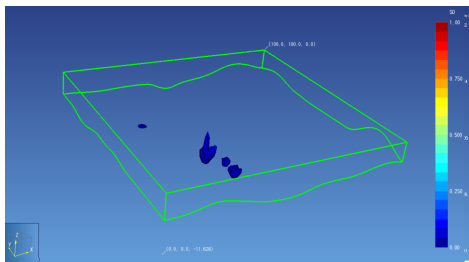
b: X-Y slice of the dissolved phase  $z = 4$  m



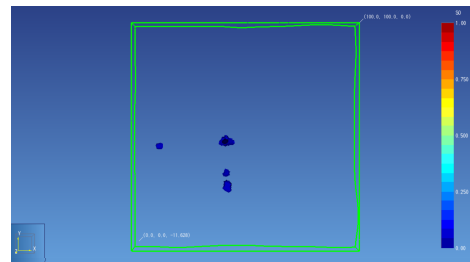
c: Area of the Dissolved phase



d: X-Z slice of the isolated  $S_{TCE}$



e: High NAPL saturation Zones side view



f: High NAPL saturation Zones upper view

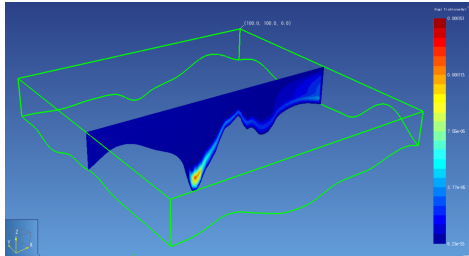
Figure 3.17. Pipe Leakage scenario. Distributed dissolved phase and NAPL position at the end of spill time

On the other hand, through analysing of the stratigraphy shape of the aquifer bed, another shallow NAPL pool is captured right beside that isolated one. The cross-sectional plane and the area of the aquifer contaminated by dissolved phase has shown in figure (3.19a) and (3.19b). AOI and  $V_{norm}$  are measured through data processing, implementing a python code. It is to remind that the Italian law has been applied for the threshold concentration

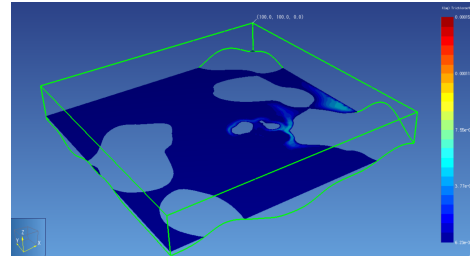
### 3.4. REFERENCE SCENARIOS

---

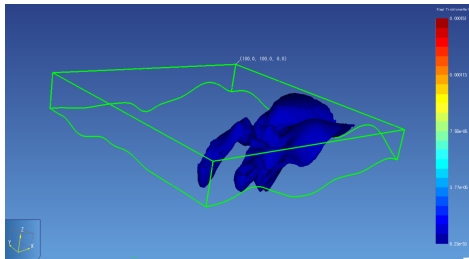
of dissolved TCE, equation (3.2).



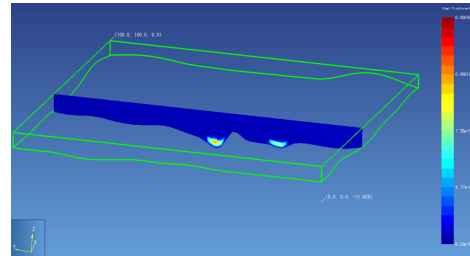
a: X-Z slice of the dissolved phase passing through the NAPL pools



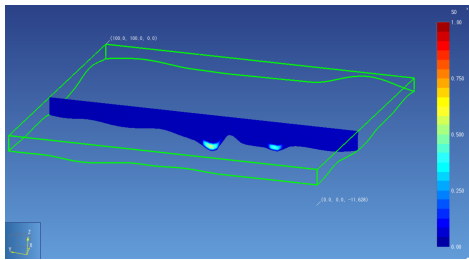
b: X-Y slice of the dissolved phase  $z = 4$  m



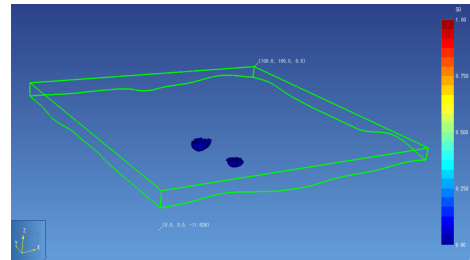
c: Area of the Dissolved phase



d: X-Y slice of the dissolved phase in the NAPL pools



e: High NAPL saturation Zones, Y-Z plane



f: High NAPL saturation Zones, side view

Figure 3.18. Pipe leakage,  $t_{monitoring} = 1$  year

After that, P&T design has been introduced by five production well, two wells directly to NAPL pool and the other three wells are positioned to contain the continuous dissolved phase. The position of well is of great importance when it comes to the producing wider cone depression. Mean

### 3.4. REFERENCE SCENARIOS

---

while the design outcomes was promising. The Max saturation of the phase has reduced form 1 to 0. Besides, the containment of the dissolved phase is captured after three months of operation, see fig (3.19). At the end of operation time , the dissolve phase volume has decreased from 3000 m<sup>3</sup> to 1428 m<sup>3</sup>. Importantly, the maximum dissolved phase molar fraction has been reduced to  $X_{TCEaq} = 1.16 \times 10^{-4}$ .

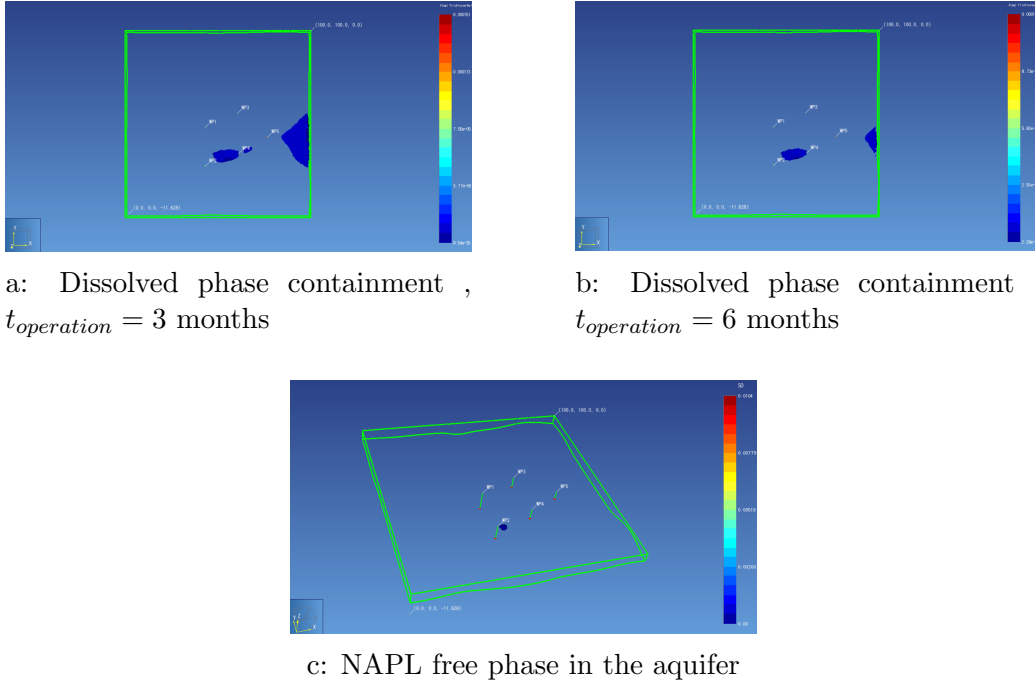


Figure 3.19. Pump and Treat Design,  $t_{operation} = 6$  months

The pump rate has adjusted between 5-8 m<sup>3</sup>/day. Note that high pumping rate with higher well completion interval is applied to the wells which are positioned to contain the dissolved phase and to create preferential pathway. Furthermore, the other two wells removes the NAPL phase directly from the generated pools. All in all, the modelling has shown promising result in application of the Petrasim for simulating of the NAPL spill behavior. The data elaboration of the output file is vital to analyse the AOI and NAPL phase occupied volume. Note that the quantification of the contaminated volume plus the graphical demonstration of the dissolve phase distribution gives an assertion about the preceding pump and treat design. However,

### 3.4. REFERENCE SCENARIOS

---

better to keep in mind that the other complementary reclamation methods are required to treat the pollution zone completely.

#### 3.4.2 Tank Spill

The tank spill of approximately 30 tons of TCE has been presumed by 4 days of seepage time and the infiltration area of  $40 \text{ m}^2$ . The ground water velocity of  $v_{water} = 0.43 \text{ m/day}$  is adjusted. Similarly, the steady state condition has been run for pressure and temperature distribution. As next step, the contaminant is injected by 24 source cells from the top of the aquifer, for period of 4 days with a mass rate of  $3.6 \times 10^{-3} \text{ kg/sec}$  see fig (3.20). Desired time intervals ranging from 3 hrs to 96 hrs are captured to observe the phenomena occurring in the system. However, as it is reported the ground velocity significantly affects the dissolve phase diffusion within the medium.

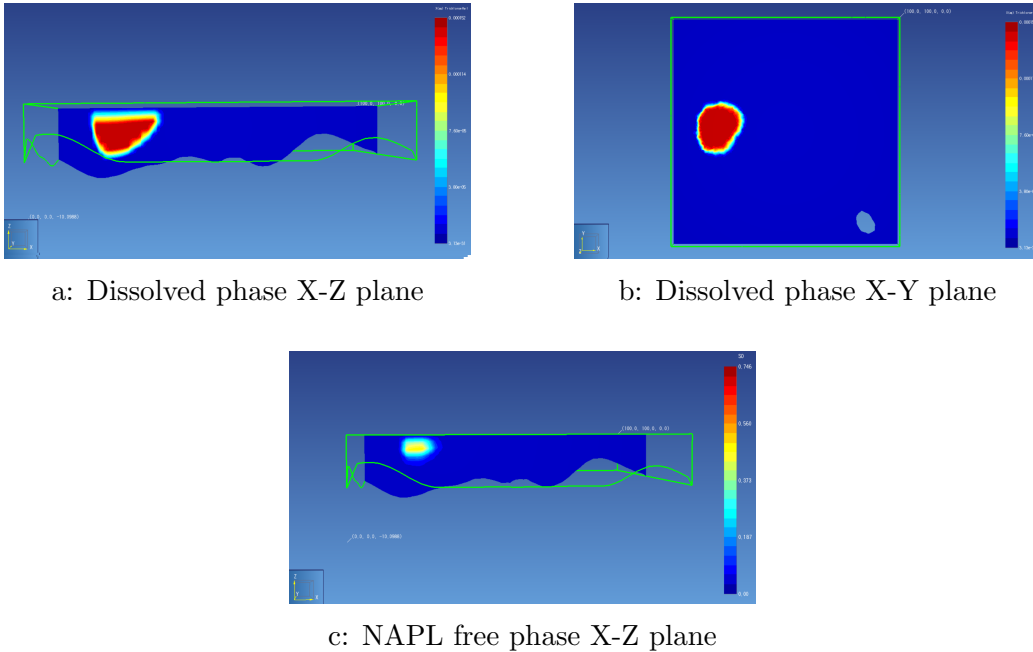


Figure 3.20. Tank spill after seepage time,  $t_{seepage} = 4$  days

### 3.4. REFERENCE SCENARIOS

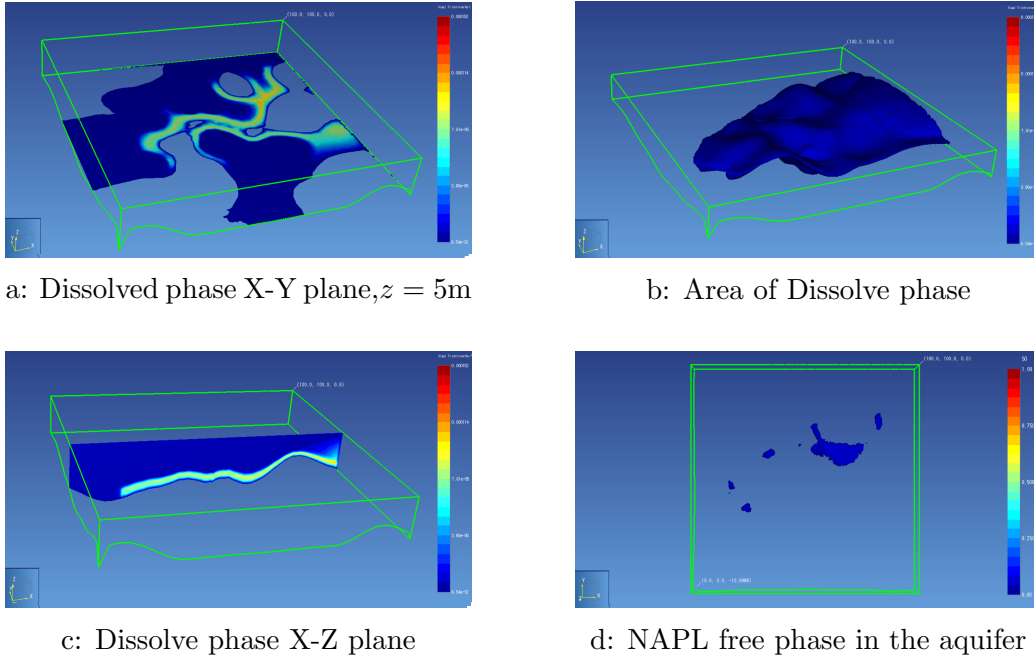


Figure 3.21. Tank spill spatial distribution at  $t_{\text{monitoring}} = 1$  year

Afterwards, the positioning of the spill after one year monitoring is obtained. As it is shown in fig (3.21), the NAPL phase and the dissolved phase spatial distribution have been captured. The irregularity of the bottom shape of the aquifer results in high diffusion of the dissolved phase within the system. Meanwhile, it is observed that the continuous generation of plume from high saturation zone is occurring. The graphical result demonstrates a massive amount of NAPL free phase which is flowing from the left side of the domain, see figure (3.22). Quantitatively, AOI and  $v_{\text{norm}}$  after the monitoring time are reported respectively  $3000 \text{ m}^3$  and .005 with max saturation of unit value. Afterwards, taking into account the spatial distribution of the free phase and the dissolved phase, pump and treat design is applied to extract the free phase as well as containment of the dissolved phase within the aquifer. Ten pumping wells are introduced by means of site reclamation, see figure (3.22). The higher pumping rate has been assigned to the wells which are to contain the dissolved phase generating larger depression cone. The operation of 6 month is assumed for the remediation plan. The implemented technique has shown successful remediation operation. The free phase is completely extracted from the aquifer, thus  $v_{\text{norm}}$  is reported zero. Besides, the area

### 3.4. REFERENCE SCENARIOS

---

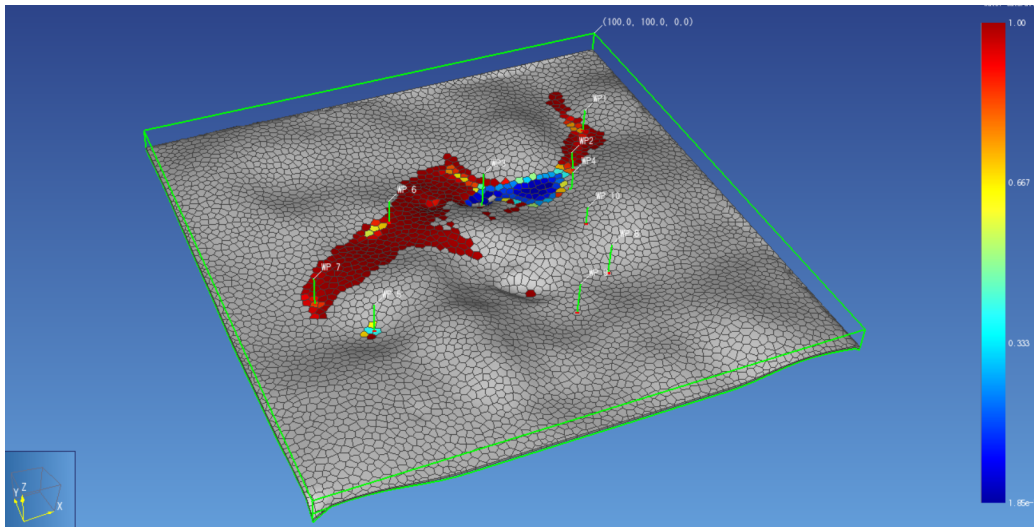


Figure 3.22. P&T design, the spatial distribution of the NAPL pool at the bottom of the aquifer at  $t_{seepage} = 4$  days

of influence has decreased to  $1183 \text{ m}^3$ . Interestingly, the maximum molar fraction of the dissolved phase is reduced to  $1.07 \times 10^{-4}$ .

All in all, it is understood that increase in the removal efficiency of the remediation plan strongly depends on the well positioning of the pumping wells. Indeed, the spatial distribution of the contamination contributes to optimization of pump and treat design.

# Chapter 4

## Conclusion

The remediation of the groundwater polluted by chlorinated solvents requires a precise examination of hydrogeological features of the subsurface system. In fact, the performed sensitivity analysis has emphasized the influence of the groundwater velocity on the spatio-temporal distribution of the DNAPL within the aquifer. Beside that, the anthropogenic parameters such as spill rate or different chemical spill are of great importance when it comes to forecasting the spreading behavior of the spill. Therefore, the spill problem necessitated the application of holistic approach to develop a remediation plan. However, the modelling of the NAPL spill has revealed practical information about the spill dynamic behavior which can be used as a tool to perform first hand remediation technique such as pump and treat. As it is demonstrated, the quantification of the relevant data such AOI and  $V_{norm}$  when combines with the spatial schematic of the contamination site, will optimize the remediation performance.

Note that the previous studies and simulations done by Petrasim have been carried out only in 2-D model domain, however the recent study has accounted for 3-D subsurface system considering a suitable degree of homogeneity and desirable boundary conditions to mimic the real underground aquifer system.

The software capability to provide practical data has been successfully tested and approved. The accessibility to the data has fortified the software capacity to incorporate different NAPL spill problem. All in all, the result of this work has shown reliability of Petrasim software for the purpose of spill modelling into the aquifer system. For the purpose of next studies, the introduction of heterogeneity of the underground water system would be recommended to be

---

addressed. Moreover, in case of larger spill amount applying non iso-thermal condition brings more accuracy to the simulation outcomes.

# Appendices

# Appendix A

## Appendix

Petrasim software prints practical output file through which it is able to extract desired parameters for further analysis of the system behaviour cell by cell.

First of all, the mesh generated file has been undergone a sorting approach, coded by Python. Then, the molar fraction of the last time step has been extracted from the file. Afterwards, following the Italian law for risk threshold concentration (CSC), the criteria (A.2) is applied to find the number of cells belonging to the interval. Through that, It is feasible to approximate the area of influence (AOI) for the dissolved phase:

$$2 \times 10^{-10} \leq X_{TCE_{(aq)}} \leq 1.51 \times 10^{-4} \quad (\text{A.1})$$

$$1.19 \times 10^{-10} \leq X_{PCE_{(aq)}} \leq 2.18 \times 10^{-5} \quad (\text{A.2})$$

---

```

#Import dependencies
import pandas as pd
import os

#opening and reading the csv file
file= open(" Directory Path " + "mesh.csv")
text= file.read()

#splitting the text file into lines
lines= text.split("\n")

#making a Dictionary as pandas input
df_dictionary= {"cell": [], "X(aq)": []}

#defining data intervals of interest
X_interval=[2e-10, 1.5e-4]

for line in lines:
    value_list= line.split(",")

    #in each ROW the 1st, 3rd, and 19th values
    #are correlated with Time step, Index of the cell,
    #and X(aq)Trichloroethyl respectively.

    if value_list[0].strip()==" End point time step (s) ":
        df_dictionary["cell"].append(value_list[2].strip())
        df_dictionary["X(aq)"].append(value_list[18].strip())
    else:
        continue

#pandas initialization
df= pd.DataFrame(data = df_dictionary)

#configuring Data types of each column
df["cell"] = pd.to_numeric(df["cell"], errors='raise')
df["X(aq)"] = pd.to_numeric(df["X(aq)"], errors='raise')

#counting the cells in the interval
counter=0
for i in range(len(df)):
    if (df["X(aq)"][i]> X_interval[0]) and (df["X(aq)"][i]< X_interval[1]):
        counter+=1

```

Figure A.1. Extraction of dissolved phase values cell by cell

To address the NAPL free phase volume, the same approach has been employed to the output file of Petrasim simulation, see figure (A.2) and (A.3). In this case, the lower cut off ratio of  $S_{VOCs} = 0.001$  is applied to build a criteria for defining the high saturation zone ( $S_{max}$ ), see criteria (A.3). After determining the number of cell, the normalized volume is achieved to illustrate which portion of the pore volume is contaminated with NAPL free phase, see equation (A.4).

$$0.001 \leq S_{VOCs} \leq S_{Max} \quad (A.3)$$

$$V_{norm} = \frac{V_{NAPL}}{V_{Porevolume}} \quad (A.4)$$

---

```

#Import dependencies
import pandas as pd
import os

#opening and reading the csv file
file= open("  Directory Path  " + "mesh.csv")
text= file.read()

#splitting the text file into lines
lines= text.split("\n")

#finding the desired data starting point
counter= 0
for line in lines:
    if line.endswith("  Desired time label (Days)  "):
        startpoint=counter
        counter+= 1
lines= lines[startpoint:]

#finding the desired data end point
indices=[]
counter= 0
for line in lines:
    if line.startswith("@"):
        indices.append(counter)
        counter+= 1
endpoint= indices[2]
lines= lines[:endpoint]

#finding the new desired data start point
indices=[]
counter= 0
for line in lines:
    if line.startswith("@"):
        indices.append(counter)
        counter+= 1
lines=lines[indices[1]+1:]

```

Figure A.2. Extraction of saturation data from the output file of Petrasim Part I

---

```

#collecting lines with data
counter=0
indices=[]
for line in lines:
    if line.startswith(" ELEM. INDEX P") or line.startswith(" (PA)") or len(line)< 10:
        indices.append(counter)
        counter+= 1

new_lines=[]
counter=0
for line in lines:
    if counter in indices:
        pass
    else:
        new_lines.append(line)
        counter+= 1

#making a Dictionary for pandas input
df_dictionary= {"So": []}

for line in new_lines:
    if len(line) > 10:
        value_list= line.split(" ")
        value_list.reverse()
        df_dictionary["So"].append(value_list[5])
    else:
        continue

#pandas initialization
df= pd.DataFrame(data = df_dictionary)

#configuring Data types of each column
df["So"] = pd.to_numeric(df["So"], errors='raise')

#defining data intervals of interest
s_interval=[0.001, df["So"].max()]

#counting the data in the interval
counter=0
for i in range(len(df)):
    if (df["So"][i]> s_interval[0]) and (df["So"][i]< s_interval[1]):
        counter+=1

```

Figure A.3. Extraction of saturation data from the output file of Petrasim Part II

# Bibliography

- [1] AE Adenekan, TW Patzek, and K Pruess. “Modeling of multiphase transport of multicomponent organic contaminants and heat in the subsurface: Numerical model formulation”. In: *Water Resources Research* 29.11 (1993), pp. 3727–3740.
- [2] Alison Alcott, Daniel Swenson, and Brian Hardeman. “Conceptual Model Tools in the PetraSim Graphical User Interface for the TOUGH2 Suite of Simulators”. In: TOUGH2 Symposium, Lawrence Berkeley National Laboratory, Berkeley, California. 2012.
- [3] Mary P Anderson, William W Woessner, and Randall J Hunt. *Applied groundwater modeling: simulation of flow and advective transport*. Academic press, 2015.
- [4] Khalid Aziz and Antonin Settari. “Petroleum reservoir simulation. 1979”. In: *Applied Science Publ. Ltd., London, UK* (1979).
- [5] Gilles Bourdarot. “Well testing: Interpretation methods”. In: (1998).
- [6] Nicholas P Cheremisinoff. *Groundwater remediation and treatment technologies*. Elsevier, 1998.
- [7] Katharina Erning et al. “Simulation of DNAPL infiltration into groundwater with differing flow velocities using TMVOC combined with PetraSim”. In: *Proc. THOUGH symposium 2009*. 2009, pp. 245–651.
- [8] FABRIZIO FRANCESCHINI. “Groundwater monitoring in environmental authorization procedures”. In: ().
- [9] Changlin Huang and Alex S Mayer. “Pump-and-treat optimization using well locations and pumping rates as decision variables”. In: *Water Resources Research* 33.5 (1997), pp. 1001–1012.

## BIBLIOGRAPHY

---

- [10] Samuel W Karickhoff and David S Brown. *Determination of octanol/water distribution coefficients, water solubilities, and sediment/water partition coefficients for hydrophobic organic pollutants*. Vol. 1. Environmental Research Laboratory, Office of Research and Development, US . . . , 1979.
- [11] Leonard F Konikow et al. “Groundwater modeling”. In: *The handbook of groundwater engineering*. CRC Press, 2006, pp. 815–866.
- [12] Douglas M Mackay and John A Cherry. “Groundwater contamination: Pump-and-treat remediation”. In: *Environmental Science & Technology* 23.6 (1989), pp. 630–636.
- [13] Robert G Maliva. *Aquifer characterization techniques*. Springer, 2016.
- [14] RJ Millington and JP Quirk. “Permeability of porous solids”. In: *Transactions of the Faraday Society* 57 (1961), pp. 1200–1207.
- [15] Federico Mondino et al. “Injection of zerovalent iron gels for aquifer nanoremediation: Lab experiments and modeling”. In: *Water* 12.3 (2020), p. 826.
- [16] RM Pitt et al. “Analysis of altered capillary pressure and permeability after thermal injury”. In: *Journal of Surgical Research* 42.6 (1987), pp. 693–702.
- [17] Michael Prats. “Thermal recovery”. In: (1982).
- [18] Karsten Pruess. “TOUGH user’s guide”. In: (1987).
- [19] Karsten Pruess and Alfredo Battistelli. “TMVOC, a numerical simulator for three-phase non-isothermal flows of multicomponent hydrocarbon mixtures in saturated-unsaturated heterogeneous media”. In: (2002).
- [20] Robert C Reid, John M Prausnitz, and Bruce E Poling. “The properties of gases and liquids”. In: (1987).
- [21] KS Sorenson, Lance N Peterson, and Tim S Green. *Evaluation of natural attenuation as one component of chloroethene-contaminated groundwater remediation*. Tech. rep. Idaho National Engineering and Environmental Laboratory, Idaho Falls, ID, 1998.
- [22] HL Stone. “Estimation of three-phase relative permeability and residual oil data”. In: *Journal of Canadian Petroleum Technology* 12.04 (1973).

## BIBLIOGRAPHY

---

- [23] Herbert F Wang and Mary P Anderson. *Introduction to groundwater modeling: finite difference and finite element methods*. Academic Press, 1995.
- [24] CL Yaws. "CORRELATION CONSTANTS FOR CHEMICAL COMPOUNDS." In: (1976).